01 Aug 2019

Bioactive Glass Fiber Fabrication Via a Combination of Sol-Gel Process with Electro-Spinning Technique

Malvika Nagrath

Adel Alhalawani

Alireza Rahimnejad Yazdi

Mark R. Towler
Missouri University of Science and Technology, mtowler@mst.edu

Recommended Citation

M. Nagrath et al., "Bioactive Glass Fiber Fabrication Via a Combination of Sol-Gel Process with Electro-Spinning Technique," *Materials Science and Engineering C*, vol. 101, pp. 521 - 538, Elsevier, Aug 2019.
The definitive version is available at https://doi.org/10.1016/j.msec.2019.04.003

Materials Science & Engineering C 101 (2019) 521–538

Contents lists available at ScienceDirect

Materials Science & Engineering C

journal homepage: www.elsevier.com/locate/msec

Review

Bioactive glass fiber fabrication *via* a combination of sol-gel process with electro-spinning technique

Malvika Nagrath[a,b], Adel Alhalawani[b,c], Alireza Rahimnejad Yazdi[b,c], Mark R. Towler[a,b,c,*]

[a] Department of Biomedical Engineering, Faculty of Engineering and Architectural Science, Ryerson University, Toronto M5B 2K3, ON, Canada
[b] Li Ka Shing Knowledge Institute, St. Michael's Hospital, Toronto M5B 1W8, ON, Canada
[c] Department of Mechanical and Industrial Engineering, Faculty of Engineering and Architectural Science, Ryerson University, Toronto M5B 2K3, ON, Canada

ARTICLE INFO

Keywords:
Biomaterials
Bioactive glass
Bioactive glass fibers
Electro-spinning
Sol-gel process
Glass precursor solution
Osteoinductive
Osteoconductive

1. Introduction

In the current state of the art, biomaterials are designed to resorb as they induce bio-activity at the host site [1]. Essentially, cell attachment and proliferation platforms, conventionally termed 'scaffolds' have been utilized for regenerative medical applications. To induce bioactivity and to facilitate resorbtion, such platforms should be contiguous with sufficient porosity to allow cell proliferation, vascularization, and transport of nutrients and metabolic waste [2]. Due to this, porous and fibrous structures are gaining popularity in tissue engineering [3]. These scaffolds are usually made from biodegradable materials (certain polymers, inorganic materials like calcium phosphate-based bioceramics and bioactive glasses-BGs) which are designed to have turnover rates comparable with the host tissue repair/restoration pace [2]. The capability of BGs to form hydroxy-apatite (HA) and resorb as they do so makes them an excellent choice as osteogenic scaffolds [2]. Bioactivity of BGs is influenced by their chemical composition and topographical features [4]. The chemical composition of these BGs is conventionally based on silicate, borate, and phosphate networks and the morphological characteristics largely depend on the fabrication method employed [4].

BGs can be fabricated using the melt-quench and sol-gel processes, resulting in various morphologies of the final glass network. Traditionally, the melt-quench technique has been used to fabricate BGs in the form of particles (like PerioGlas®, NovaBone Products, LLC., Alachua, Florida, USA) and monoliths (such as the middle ear prosthesis, MEP®, US Biomaterials, Alachua, FL, USA) [4,5]. The bioactivity of melt-quench BGs is dependent on composition rather than texture [6]. With the advent of the sol-gel process of glass fabrication, an additional advantage of various morphological textures can be induced in the otherwise non-textured melt-quench derived BGs [4].

Constructs with one of the dimensions in "nano" range (One-dimensional, 1D, nanostructures) like fibers, wires, films and, coatings have received attention in the electronics, photonics, mechanics, sensing and biomedical fields [7–11]. Of the various techniques available to fabricate 1D nanostructures, electro-spinning (ES – *the abbreviation will be used for the words electrospin and electrospun*) has become popular because of its simplicity, versatility, ease of the procedure and low cost of fabrication [12]. ES of BGs in combination with the sol-gel process is becoming increasingly popular [13]. ES fibers have been used for drug delivery, wound healing, vascular grafts and scaffolds [12,14–16].

It is evident from the literature that the sol-gel process can provide a porous and fibrous architecture to BGs [4,5,17,18] and ES is used to draw submicron dimensioned polymer fibers for biomedical

Abbreviations: BGs, Bioactive glasses; HA, Hydroxy-apatite; SBF, Simulated body fluid; GPCs, Glass Polyalkenoate Cements; ES, Electro-spinning/Electrospin/Electrospun; MBG, Mesoporous Bioactive Glass; ECM, Extracellular Matrix; TASG, Template-Assisted Sol-Gel; GPS, Glass precursor solution; P123, Pluronic123; PVP, Polyvinylpyrrolidone; TEOS, Tetraethyl orthosilicate; PVA, Polyvinyl alcohol; PEO, Polyethylene oxide; PVB, Polyvinyl butyrate

* Corresponding author at: Mechanical and Industrial Engineering, 350 Victoria Street, Toronto, ON M5B 2K3, Canada.
E-mail address: mtowler@ryerson.ca (M.R. Towler).

https://doi.org/10.1016/j.msec.2019.04.003
Received 2 October 2018; Received in revised form 28 March 2019; Accepted 1 April 2019
Available online 03 April 2019
0928-4931/

engineering applications [12,14,15]. The fabrication of nano-dimensioned BG fibers combining sol-gel process and the ES has been demonstrated by the scientific community [13,19–22]. The literature provides extensive illustrations of the use of ES for polymers; ES of BGs essentially works on the same principles as for the polymers [8], but certain alterations (like the addition of polymer to the sol) to the process are required. The focus of this paper is to elaborate on the process of BG fiber production using a combination of the sol-gel process with ES. The present paper also aims to review various factors affecting this process, the morphology of the fabricated BG fibers, their bioactive performance, and cellular response.

2. Glass fabrication methods

BGs can be fabricated using the melt-quench and the sol-gel processes, resulting in various morphologies of the final glass network.

2.1. Melt-quench technique

Glasses have traditionally been made by the melt-quench technique [23]. Early BG formulations like Bioglass® were prepared by melt-quench in both particulate and monolithic form [4,5]. The technique involves heating the precursors to high temperatures (usually around 1450 °C for silicates) and then quenching them in water to fabricate glasses [24–26].

2.2. Sol-gel process

In the 1980s there was a shift in fabrication methods towards the sol-gel approach [23], meaning that the preparation of glasses in fiber and foam forms for use as porous scaffolds, coatings and net shape monolithics are now a possibility [4,5]. As compared to the melt-quench technique, the sol-gel process allows the fabrication of glasses at low temperature, where the hydrolysis and condensation of organometallic precursors is followed by ageing of the sol which leads to the formation of a gel that is heated (up to 700 °C) during the calcination process [19,24–26].

Generally, the sol-gel process for glasses includes several controlled steps which have been described in detail in the literature [23,27]. Modifications to the sol-gel process (such as addition of surfactants as templates, use of co-solvents and swelling agents to tailor such textures [2,21,28]) are usually applied to retain network porosity [27] which provide advantages of high specific surface area, protein adsorption, and cell seeding in the 3D architecture. Mesoporous bioactive glass (MBG) powders are one of the examples of such modification. These MBGs have proved themselves to have a higher specific surface area and pore volume as compared to BG powders, which is a predictor of enhanced bioactivity, osteogenesis and drug loading/delivery [6].

3. Bioactive glass scaffolds

Scaffolds for tissue engineering purposes are expected to provide temporary platforms for cells to synthesize new tissue. An ideal scaffold should be biocompatible, biodegradable, bioactive, have specific architecture, and mechanical properties [2,29,30]. BGs are osteoconductive and osteoinductive and have already been advanced as commercial products [4,5,29] such as silicate particulates for both bone regeneration (like PerioGlas®, NovaBone Products, LLC., Alachua, Florida, USA), and treating tooth hypersensitivity (NovaMin®, NovaMin Technology, FL, owned by GlaxoSmithKline, UK since 2010) [4,5] and a borate-based product (such as Mirragen™ by Avalon Medical, USA) [31]. But the inherent brittleness and challenging manipulation of BGs to form 3D constructs have warranted the fabrication of their composite (BG + polymer) structures [29,30]. Addition of BGs to polymers enhances their bioactivity and mechanical strength and allows for the construction of 3D scaffold of inherently brittle BGs as well [29,30,32]. Melt-quench and sol-gel processes have been utilized to fabricate BG scaffolds [2], and both processes have their advantages and disadvantages [4,5,18,23–25,33,34]. The architectural requirements for a scaffold include having a 3D porous structure with a degradation rate comparable to the restoration pace of the tissue being repaired. Generally, pores of 100 μm or greater with > 50% porosity are minimum requirements for a scaffold and melt-quench glass constructs usually suffer from narrow porosity ranges and constricted connectivity between neighbouring pores [2]. The scaffolds prepared through the sol-gel process display a hierarchical pore structure which imitates the arrangement of the natural tissue [2]. These scaffolds show better biomineralization due to faster dilution of ions because of the higher surface area. However, they have lower strength (2–3 MPa) when compared to melt-quench glass-based scaffolds (up to 140 MPa) [2].

3.1. Bioactive glass fibers

The application and performance of BGs are dictated by their morphological and structural properties [22]. ES is a simple, low cost and versatile technique to fabricate submicron fibers, usually employed for manufacturing polymers for medical applications [12,14]. The technique is also used to formulate composite (BG + polymer) fibrous scaffolds using multiple combination techniques [32,35–38]. An advantage of the sol-gel process is that its inorganic sol can also be fed into the ES apparatus to fabricate glass fibers [21,24]. Increased applications of nanotechnology in the biomedical field has brought focus to the novel technique of ES [12,14,19,39]. ES non-woven nanofibrous matts can mimic the extracellular matrix (ECM, the native environment of the cells) and provide a physiological environment in which cells can regenerate [2,4]. These fibers possess high specific surface area, have tunable porosity, and surface functionalization can be imparted to them [15].

3.1.1. BG fibers from melt-quench glasses

45S5 Bioglass®, a conventional melt-quench derived silicate BG, cannot be sintered and/or drawn into fibers using melt-spinning (usually used for drawing non-BG fibers) without crystallizing the structure [3,4,40]. Melt-spinning involves drawing fibers from the melts of the glass (either directly from raw materials or indirectly from the prefabricated glass marble) extruded through platinum alloy bushings of various diameters and then solidifying the extruded glass before crystallization can occur [41]. Structural development *via* melt-spinning depends upon the interaction of rheological properties, heat transfer, and crystallization kinetics of the solution [42]. The melt-spinning process leads to devitrification of Bioglass® [40] due to its narrow sintering window [4]. However, researchers have overcome the problem of crystallization of 45S5 BG when fibers are drawn from the material using a laser spinning technique [3]. Clupper et al. [43] analyzed the crystallization kinetics of tape cast 45S5 BG *via* non-isothermal methods; they concluded that the surface crystallization phenomenon was dominant, and the structure was fully crystalline before undergoing significant densification at 800 °C.

3.1.2. BG fibers using sol-gel process

The sol can be fed into ES equipment [24] facilitating the fabrication of submicron glass fibers which can be manipulated electrostatically and assembled in ordered structures [7]. These ultrathin fibers have homogeneous composition distributions [7,13], possess up to three times the specific surface area when compared to thicker melt-quench glass fibers [20] (Fig. 1), and allow for inorganic/organic composite and ceramic constructs' fabrication [8]. The comparison of the silica sol-gel MBG (300 m^2/g and 4.4 nm) [6] with silica sol-gel/ES nanofibrous matt (285 m^2/g and 3.8 nm) [21] was considered in terms of their specific surface area and pore size; it was noted that, although MBGs offer higher specific surface area and pore size, ES fibers can provide the architectural benefit of ECM.

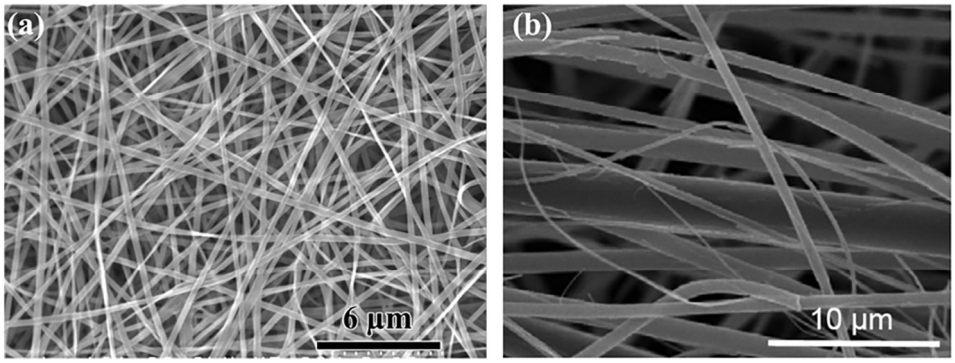

Fig. 1. (a) Sol-gel-ES BG fibers with a diameter in the range of 100–450 nm. (b) Melt-quench derived BG fibers with a diameter in the range of 100–800 nm [2].

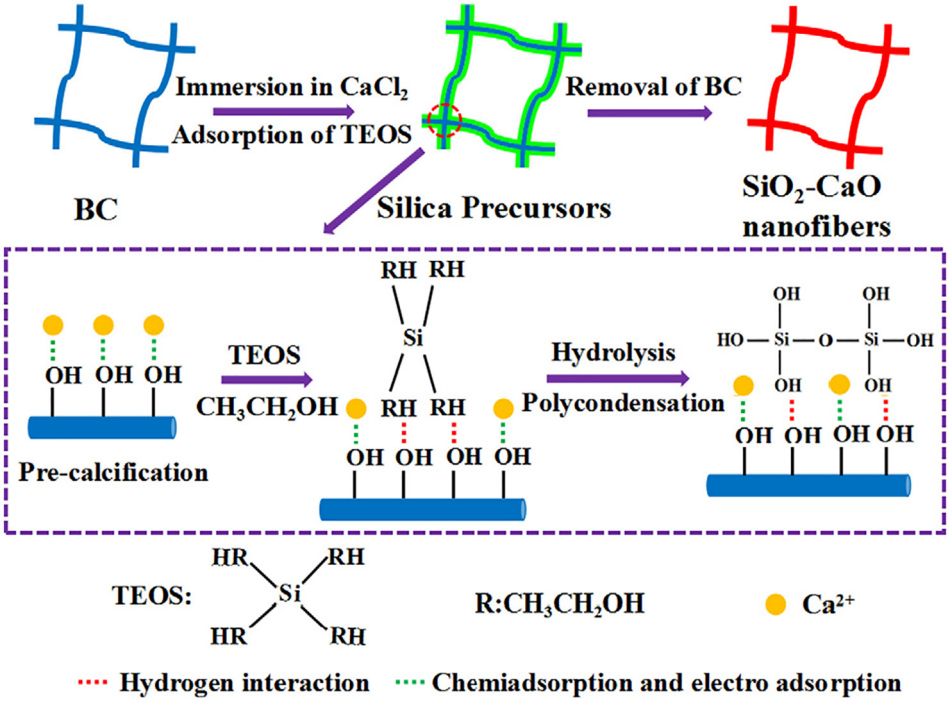

Fig. 2. Template assisted sol-gel process [45].

Researchers are also employing other techniques to formulate BG fibers using sol-gel method along with the sacrificial template [44,45], fiber drawing, or spraying processes [46,47]. Luo et al. [44,45] used bacterial cellulose aerogel as a template which was immersed in the sol [44,45]. Removal of the organic component and calcination of the BG was achieved by thermally treating the immersed aerogel [44,45]. The template assisted sol-gel process (TASG) for manufacturing BG fibers is shown in Fig. 2. Generally, the diameter of the ES fibers [13,21,22,48] was found to be higher than the TASG fabricated fibers [44,45]. The average diameter of the BG fibers can be controlled with the design of the template and immersion time [44,45]. The fiber diameter and percentage porosity were compared for TASG ($60SiO_2$-40CaO mol%) [45] and sol-gel ES BG fibers ($70SiO_2$–30CaO mol%) [48]. The fibers made *via* TASG [45] could provide thin diameters (~29 nm after 6 h of immersion in tetraethyl orthosilicate,TEOS and ethanol mixture) as compared to sol-gel ES BG fibers (300 nm) [48], but the extent of porosity was found to be higher for ES (89.7%) [48] than TASG (63.8%) [45]. For the same set of fibers, it was also noted that the specific surface area of TASG BG fibers [45] was much higher than the sol-gel ES fibers made without the addition of surfactant to their composition [48]. The mesopore diameter and the specific surface area of the TASG [44] and sol-gel-ES BG fibers [13] were also compared. The mesopore diameter of TASG BG fibers ($60SiO_2$–36CaO-$4P_2O_5$ mol%) was 39.4 nm [44], while the ES fibers ($70SiO_2$-25CaO-$5P_2O_5$ mol%) [13] were shown to have mesopores diameters in various ranges (3–5 nm, 3–16 nm, 32–65 nm, Fig. 3). Multiple ranges of mesopores diameters can be designed by the addition of surfactant P123 and by controlling the shrinkage of the as-spun fibers [13] (as-spun fibers have been defined in Section 5). After comparing the specific surface area reported by these studies [13,44], it was found that ES fibers are capable of providing a higher specific surface area (141 m^2/g for the fibers with 32–65 nm range diameter mesopores) [13] than TASG fabricated fibers (127.4 m^2/g for the fibers with 34.9 nm diameter mesopores). Luo et al. also manufactured the BG-gelatin composite using the template method to improve the biological and mechanical properties of the scaffold [49].

Oréfice et al. [46] have demonstrated the fabrication of continuous and discontinuous BG fibers by both drawing and spraying processes using the sol (Fig. 4). In these processes, the formed sol is drawn or sprayed *via* orifices in the sol reservoirs under pressure [46]. The formation of continuous, discontinuous, and "glass-wool" morphology has been reported by this technique [46]. One of the major advantages of using sol-gel processes and fiber morphology is the resultant increased specific surface area [46]. The specific surface area and pore volume of

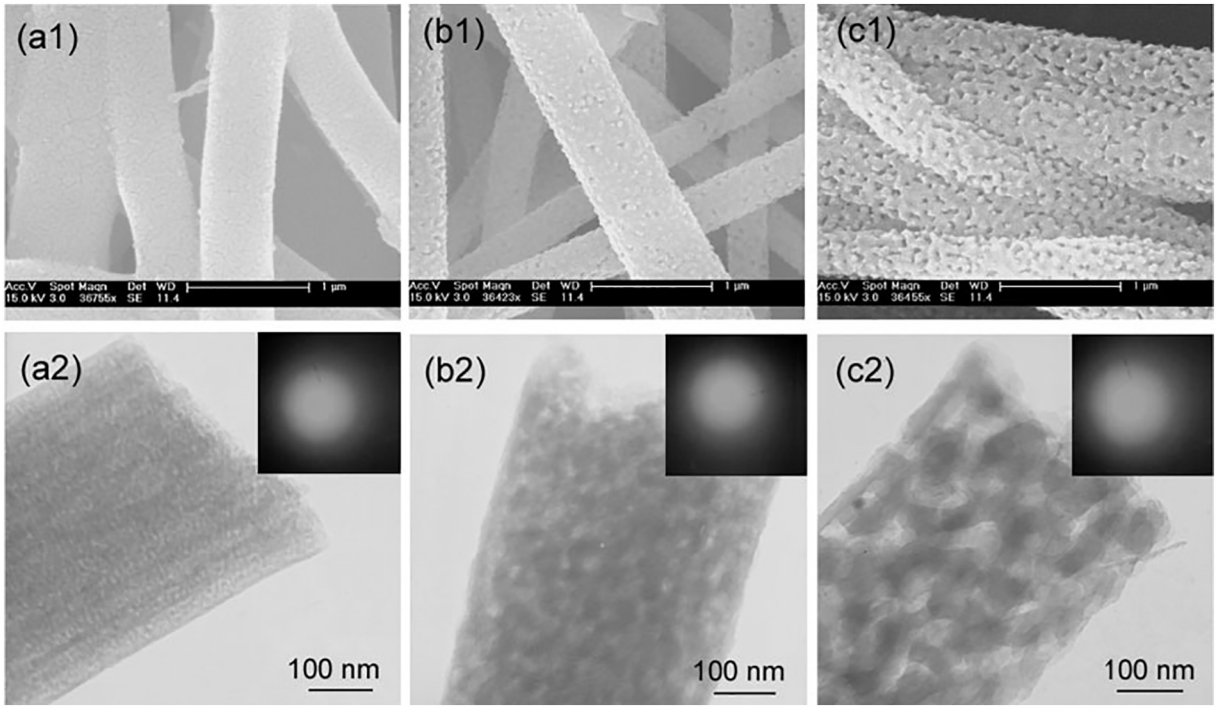

Fig. 3. Sol-gel-ES BG fibers ($70SiO_2$-$25CaO$-$5P_2O_5$ mol%) with mesopores diameters in various ranges (3-5 nm, 3-16 nm, 32-65 nm). SEM images - a1, b1, and c1; TEM images - a2, b2, and c2. The insets (Electron Diffraction patterns) show these fibers are amorphous [13].

the fibers were found to be lower than the sol-gel fabricated monoliths [46]. The reported specific surface area of the fibers was 50 m^2/g (heat treated at 180 °C) while the sol-gel made monolith showed higher values (200 m^2/g) with the same processing variables [46]. Another study [47] also fabricated sol-gel fibrous mesh by spraying and collecting the fibers (of the sol) through a spraying assembly under pressure. They also reported a lower specific surface area (2 m^2/g) of the fibers as compared to the sol-gel formed powders with the same composition and processing conditions [47].

4. Electro-spinning

4.1. Process

Fundamentally, the ES equipment (Fig. 5a) contains a syringe and a pump (to deliver the solution), a high voltage power supply (to be applied on the syringe tip/spinneret), and an electrically conductive collector (to collect fibers). For the fabrication of fibers, ES relies on electrostatic interactions (between electrically charged ES solution and

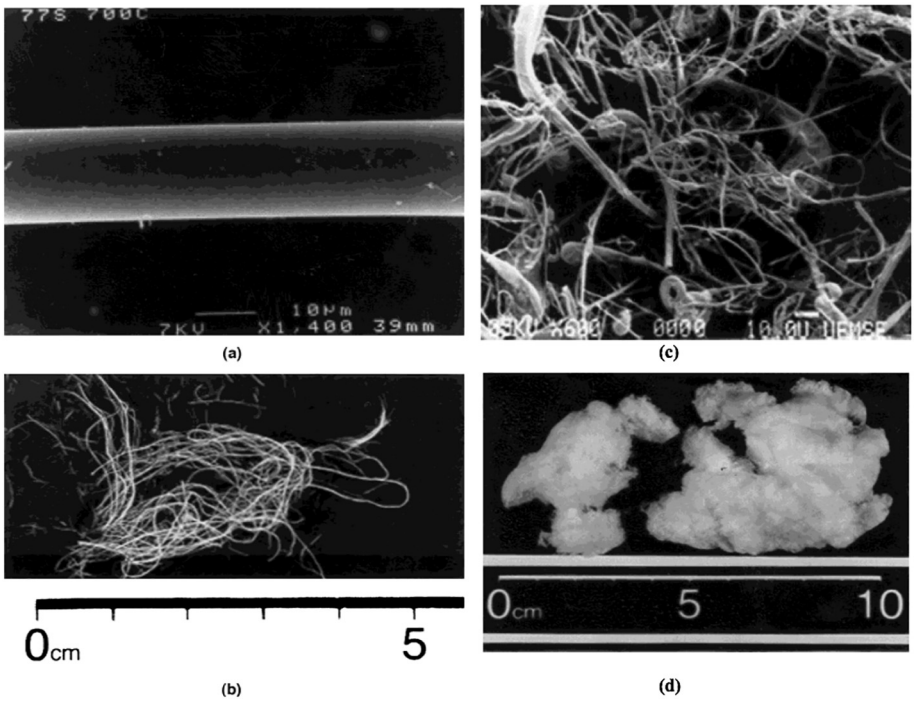

Fig. 4. Continuous (a-SEM and b-optical image) and discontinuous (c-SEM and d-optical image) BG fibers made by drawing and spraying of the sol [46].

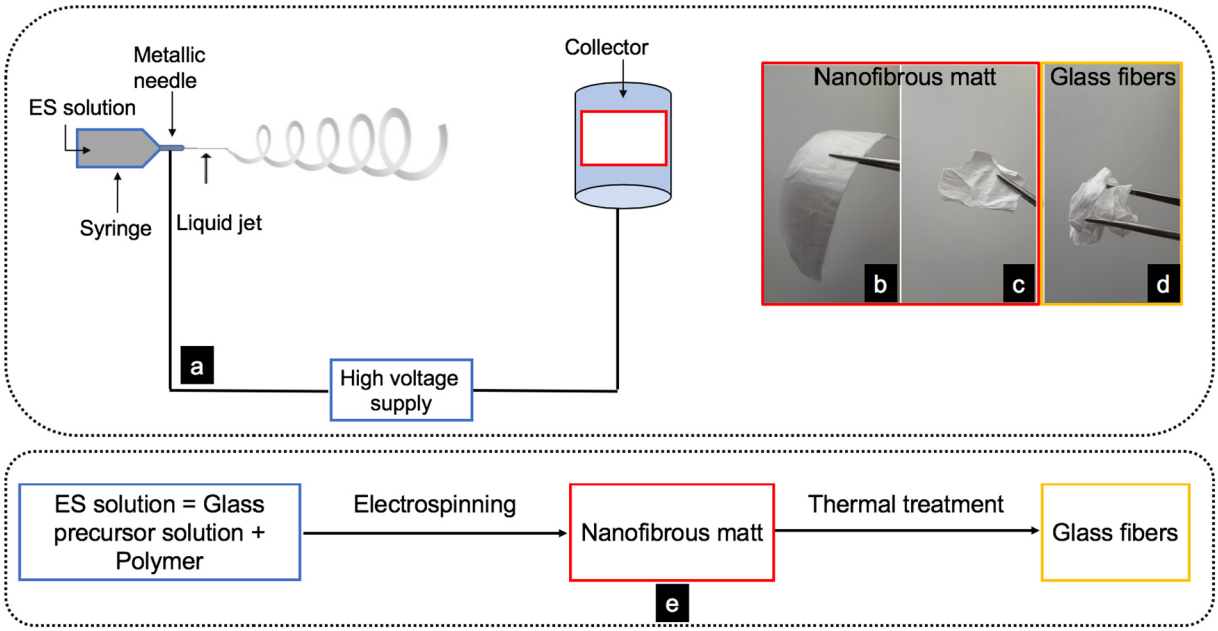

Fig. 5. a-Fundamental setup of ES equipment: syringe, high voltage supply, and an electrically conductive collector. Optical images of the ES BG fibers before (b and c) and after (d) thermal treatment [56], e-usual process of ES of BGs. The process steps have been color co-ordinated with respective picture outlines.

oppositely charged collector, and within the ES solution) rather than mechanical stretching of the material [7]. The drop of charged solution (at the syringe tip) with optimum viscosity is suspended under high voltage electric current to overcome the surface tension of the liquid. Because of the electrical charge, the drop changes from a spherical to a more conical shape called a Taylor cone [7]. A jet is ejected from the tip of the Taylor cone when the surface tension of the drop is overcome by the strength of the electric field. As a result of rapid bending and whipping processes in the electrified jet, it is continuously stretched and elongated by electrostatic repulsive forces leading to the formation of ultrathin fibers [7]. This jet is collected on the grounded target collector (set up at a distance) in the form of a solid filament dried by evaporation of the solvent during its flight from the cone to the collector [7–10,19,50–55]. The presence of chain entanglements in the solution with adequate viscosity within the charged solution (usually a polymer) does not allow it to break up into droplets/particles (seen for low viscosity solutions for electrospraying) [8] and a continuous non-woven fiber is laid down on the target [16].

5. Glass Electro-spinning

One of the most important parameters that affect ES is the rheological behaviour of the solution [26]. The process of ES for polymers is similar for BGs with certain modifications because the rheological properties of glass precursor solutions (GPS) are dissimilar to those of polymers [17,48]. ES relies on the use of an optimal GPS [20] which should have sufficient intermolecular interactions and chain entanglements for the fibers to be drawn. Usually, the glass producing liquid is mixed with a polymer (Fig. 5e) containing long chains to provide intermolecular interactions which facilitate fabrication of fibers *via* ES [17,48]. Addition of the polymer to the GPS provides adequate intermolecular interactions for the solution to ES. The 'as-spun' nanofibrous matt (polymer + GPS) (Fig. 5b and c) then undergoes calcination (Fig. 5e), sintering or chemical conversion from the precursor to the final glass matrix and removal of organic components [17,48] (Fig. 5d).

5.1. Role of polymers in the Glass ES

Theoretically, ES of the BGs can be achieved from inorganic sol at high temperatures without adding the polymer (termed as 'inorganic sol ES') [20]. The GPS/inorganic sol (sol-gel process) are thermostatically unstable systems [7] with high fluidity and low viscosity due to insufficient intermolecular interactions [57], and ideally, a material with long chains in a volatile solvent can be ES [58]. Sufficient intermolecular interactions are necessary for a solution to be ES because the chain entanglements allow for the fibers to be drawn when an electric field takes over the surface tension of the liquid droplet [50]. Therefore, the addition of the polymer with long chains is required to draw fibers using ES (known as 'polymer assisted ES') [57].

Generally, a solution with adequate viscosity is required for ES. However a study by Madhugiri et al. [59] reported the use of gel forms of GPS to undergo the process. It is important to find the optimum spinning window for the viscosity of the solution by addition of the appropriate concentration of the polymer [26]. Rheological properties of the GPS can be controlled in polymer assisted ES. Xia et al. [57] explained that the type of polymer used influences the viscosity, elasticity, and electrical conductivity of the solution along with conformation of the polymer chains, hence influencing the fiber diameter.

Adding more than one polymer in the GPS can alter the viscosity, surface tension and electrical conductivity of the solution, which influences the fiber morphology and diameter to a limited extent [57]. To analyze the effect of an additional polymer in the spinning solution (GPS + polymer), Xia et al. [57] added P123- Pluronic 123 (polyethylene oxide, $PEO)_{20}$ – (polypropylene oxide, $PO)_{70}$ - PEO_{20}); a nonionic triblock copolymer– (at the expense of GPS) to the mixture already containing polyvinylpyrrolidone (PVP) in various concentrations. They found that the fiber diameter reduced as the concentration of P123 was increased from 0 to 0.27 g/ml; above this concentration, the fiber diameter increased again [57]. Though Xia et al. [57] used P123 as a supplementary polymer in their study, it is used as a surfactant in other BG fiber productions *via* ES [13,21], so it is difficult to say whether this effect is the result of supplementary polymer or surfactant. This result can also be due to the reduction of GPS in the final, spinnable solution, as altering the concentration of GPS affects the morphology of fibers [20,60]. The concentration of used P123 in these studies [13,21,57] is also noteworthy. When used as a supplementary polymer in the concentration between 0 and 0.27 g/ml, it is reported to have an effect on the diameter of the fibers [57], but when used as a

surfactant to induce porosity on the fibers, it is used in the concentration of about 0.023 g/ml [13,21]. This aspect needs further investigation to determine the concentration-dependent effect of P123 on the BG fibers.

5.2. Regulation of hydrolysis and gelation of inorganic sol

When ES, the hydrolysis and condensation of silicate precursor, TEOS and inorganic sol, in general, have to be controlled so that the gelation does not take place and the solution can undergo ES [60]. Some studies regulated hydrolysis and gelation by monitoring the viscosity of inorganic sols [19,58,61], and others added surfactants and structure forming agents [59]. Addition of the surfactant and surface forming agents can endow porosity in the final structure along with controlling the hydrolysis and gelation of the inorganic sol [59], while their absence leads to solid fiber fabrication [19,58,61].

5.3. As-spun fibers

The as-spun fibers containing a surfactant in their GPS compositions do not show stability when positioned on the relaxant surface (after being peeled off from the assembling support surface such as copper wire drum or aluminum foil), they tend to coil and shrink [13,21]. The fibrous shrinkage is attributed to the axially aligned surfactant molecules with high conformational entropy [13]. Studies have shown that by controlling this shrinkage, the pore size after the heat treatment can be regulated [13,21]. After the non-woven ES fibrous matt has been generated, this structure undergoes thermal treatment for the calcination of the glass and burn-out of the residual polymer [20,57].

5.4. Post-ES thermal treatment

Polymer assisted ES studies reported heat treatment in the range of 600–700 °C for 3-5 h (h) [13,20–22], while inorganic sol ES studies reported thermal treatment around 60 °C for 12–72 h [19,58]. Other studies using inorganic sol ES have reported no thermal treatment at all for silicate fibers [61,62]. The studies [61,62] with no thermal treatment reported have used TEOS as the silicate precursor along with water, acid and ethanol. TEOS is a silicon alkoxide precursor which undergoes hydrolysis and condensation reaction (catalyzed by acid or base) in the presence of water and organic solvent (usually an alcohol) to form Si-O-Si linkage and volatile alcohol [27]. The organic solvent is usually chosen same as the anticipated side product of the condensation reaction (ethanol in this case) to avoid mixing of alcohols [27]. In the cases of thermal treatment, as a result of the calcination, the BG fibers undergo morphological changes in terms of their diameter, linear shrinkage, weight reduction, and propensity to crystallize.

5.4.1. Reduction in the diameter

Generally, reduction in the fiber diameter is related to the loss of polymer as a result of post-ES thermal treatment (Fig. 6) [17,20,57]. However, the morphology is maintained similar to as-spun fibers [17]. Heat treatment reduces the fiber diameter by a factor of 2–3 [17,20]. Kim et al. [20], and Xia et al. [57] reported a reduction in the diameter of the calcined fibers compared to as-spun $70SiO_2$-$25CaO$-$5P_2O_5$ mol% and BG fibers comprising of SiO_2-CaO-P_2O_5 network (the composition of BG is not mentioned in the article), respectively. While Hong et al. [21] showed that calcined silica fibers were of similar diameter to that of as-spun fibers. All reported compositions [20,21,57] were calcined in the range of 600–700 °C for 3–5 h decomposing the polymers and nitrates from the precursors. It can be inferred that, when used alone, the silica network can retain the as-spun fiber diameter, but when Si, Ca, and P compositions are used, the glass network is modified by the additional network former and modifier leading to the reduction in diameter of the fiber as compared to as-spun fibers.

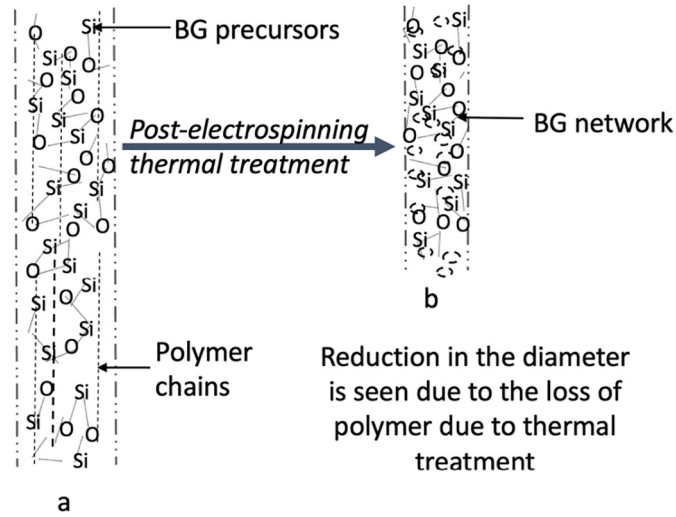

Fig. 6. Diagrammatic illustration of the reduction of fiber diameter post-ES thermal treatment (adapted from Gao et al. [60]). a- As-spun fiber containing polymer and GPS; b- fiber with reduced diameter after thermal treatment due to decomposition of polymer from GPS.

5.4.2. Linear shrinkage

Xia et al. [57] and Hong et al. [21] used P123 as a supplementary polymer and surfactant in BG fibers with SiO_2-CaO-P_2O_5 network (the composition of BG is not mentioned in the article) and silica fiber GPSs' compositions respectively; Kim et al. [20] did not add any surfactant to their GPS composition ($70SiO_2$-$25CaO$-$5P_2O_5$ mol%). Studies which used P123 [21,57] reported shrinkage of the calcined fibers in the longitudinal direction as compared to as-spun fibers (Fig. 7), while the study without P123 [20] did not report fiber shrinkage linearly after calcination. It can be concluded that the linear shrinkage in BG fibers post-ES thermal treatment occurs in the presence of surfactant P123 and it is due to the micellization of this surfactant.

5.4.3. Weight reduction

Studies have shown weight loss of the fibers with heat treatment [62]; attributable to the evaporation of solvents, decomposition of the polymer, and self-condensation reaction of silanol groups [62]. 60 wt% reduction in the $29.4SiO_2$–$37.14CaO$-$32.06P_2O_5$–$1.66MgO$ wt% fibers (about the removal of polymer and alkoxides) was reported between 270 and 600 °C, while no significant weight reduction was noticed at higher temperatures [63].

5.4.4. Crystallization of the glass

BGs are amorphous in nature, and elevated thermal treatment temperatures can devitrify them. The degradation of the BGs is hindered by the development of crystals; crystallization is not required for the degradable scaffolds. Studies have reported the formation of crystals when as-spun fibers are heat treated at temperatures higher than 700 °C [63]. Asgharnia et al. [63] reported the formation of bioactive-glass-ceramic fibers with HA crystals at temperatures higher than 800 °C of $29.4SiO_2$–$37.14CaO$-$32.06P_2O_5$–$1.66MgO$ wt% GPS with PVP fibers. X-ray diffraction (XRD) peak intensity for HA was seen to amplify by increasing the temperature to 950 °C. The fibers were also found to be no longer smooth due to the presence of HA nanoparticles [63]. It was anticipated that probable rise in temperature from 700 °C to 950 °C causes the mechanism of crystallization in the glass network which converts glass fibers to glass-ceramic fibers [63]. These results conclude that thermal treatment temperature should be selected to maintain the amorphicity of the glasses.

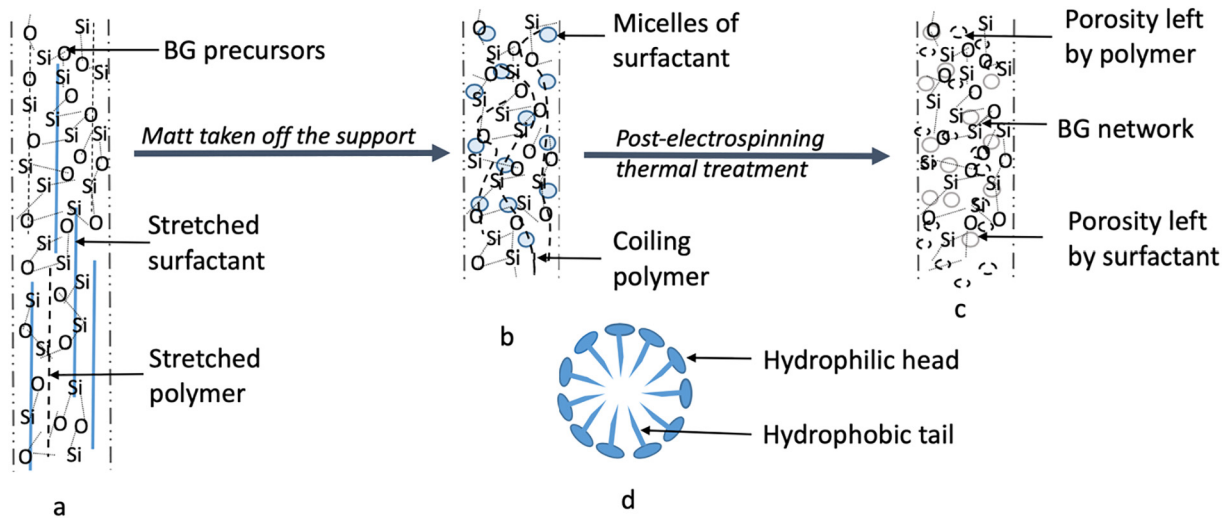

Fig. 7. Diagrammatic illustration of the linear shrinkage post-thermal treatment (adapted from Gao et al. [60]). a- As-spun fibers on the support (usually Al foil); b- As-spun fiber taken-off the support leading to the orientation of surfactants in micelles and hence linear shrinkage; c- BG fibers after thermal treatment depicting BG network and porosity left by decomposed fibers and surfactants; d- a micelle depicting hydrophilic head and hydrophobic tail.

5.5. Benefits of ES BG fibers

The nanofibrous nature of the BG structure provides benefits of high specific surface area, small pore sizes in the deposited matt, and the possibility of assembling the matts in desirable 3D macro-porous constructs [13,22] (Fig. 8). Polymer fibers formed *via* ES usually fall in the range of 100 nm to 5 μm in diameter [50,64]. Glass fibers drawn using a mechanical fiber spinning and melt-spinning technique possess higher diameter (in the micrometer range) compared to ES fibers [17,20,57]. Due to their high specific surface area, ES BG fibers exhibit increased bioactivity over fibers fabricated *via* mechanical spinning [57]. The high specific surface area allows for the rapid dissolution of ions, higher protein absorption [60], controlled drug delivery [13,22] and osteogenic potential [20,60] enhancing the bioactivity of these ES constructs. Another advantage of the fibrous matts fabricated with ES is that loosely assembled fibers allow for nutrient distribution and angiogenesis [65]. Attempts to induce porosity [13] and hollowness [22] within the fibers are prompted to further boost the surface area of the ES fibers [13,22]. These alterations can provide the benefits of increased drug loading and superior bioactivity [13,22].

Due to the stated benefits of the ES BG fibers, they have been directed towards protein adsorption [21], bone regeneration [13,17,19,20,26,57,58,60,66], hard tissue repair [22,48], drug delivery [13,22,66], wound healing [13,22], and fibrous templates [62] (Table 1).

5.6. Morphological changes in ES fibers

The morphology of ES fibers can be dependent upon:

a) *Process variables* – electric field strength, fluid flow rate, and working distance between electrodes,
b) *Solution variables* – viscosity, electrical conductivity, surface tension, and solvent volatility, and
c) *Environmental variables* – temperature, pressure, and humidity [67].

For polymers, all of these parameters have been extensively described and researched in the literature [12,14,16] An undesirable feature in the form of beads can be seen on the surface of the ES fibers [68]. The viscosity of the solution, the net charge density of the jet and surface tension of the solution are the main factors affecting the presence (or absence) of beads on the surface of fibers [68]. These beads provide non-uniformity to the fibers and are very difficult to remove. Lower surface tension, higher viscosity and higher net surface charge density favour the absence of beads from the fibers [68]. The balance between surface tension and viscosity of the solution with adequate electric field strength are required for the uniform fiber ejection [68]. Table 1 enlists various factors studied with respective glass compositions in different journal articles.

5.6.1. Effect of viscosity

It is one of the critical factors to be considered for ES of any solution. Generally, the higher the viscosity of the polymer solution, the lesser the presence of the beads on the fibers and the higher the diameter of the resultant fibers [16,64,68]. With increasing the viscosity, beads change their form from spherical to spindle-shaped; over time they will eventually disappear [68]. Mckee et al. demonstrated that the uniformity of the ES fibers is not dependent on the molar mass of the polymer; sufficient intermolecular interactions (within the polymer solution of high or low molar mass) that can effectively act as chain entanglements are essential [50]. But reviewing other studies [21,57], it is evident that the molecular wt of the polymer is an important parameter towards viscosity of the solution (Section 5.6.2).

Lu et al. [48] and Poologasundarampillai et al. [58] reported viscosity of about 1 Pa·s and 0.56–0.95 Pa·s optimum to ES 70SiO_2–30CaO mol% fibers with polymer-assisted polyvinyl alcohol (PVA) and inorganic sol ES with resultant fibers in the range of 300 nm and 1.5 ± 0.4 μm diameter, respectively. These studies lead to the observation that reduction in the viscosity of the solution leads to the reduction of the diameter of the BG fibers.

5.6.2. Effect of the concentration of the polymer solution

Adequate polymer concentration which provides sufficient chain entanglements and intermolecular interactions are required to achieve uniform fibers without beads, but higher than optimal polymer concentration leads to viscous and unspinnable solutions [13,57]. Also, as the concentration of the polymer is increased, the diameter of the fibers also increases [57]. Hong et al. [21] and Xia et al. [57] ES silica and BG fibers with SiO_2-CaO-P_2O_5 network (the composition of BG is not mentioned in the article) with the addition of polyethylene oxide- PEO (average molecular wt = 2,000,000) and PVP (average molecular wt = 45,000) respectively. Xia et al. [57] concluded that a lower polymer concentration of 0.2 g/ml (20 wt%) resulted in unstable fibers, and as the concentration of the polymer increased, the diameter also increased. Hong et al. found they could ES the GPS with the addition of low wt% of polymer (0.8–1.8 wt%) as compared to Xia et al.; the

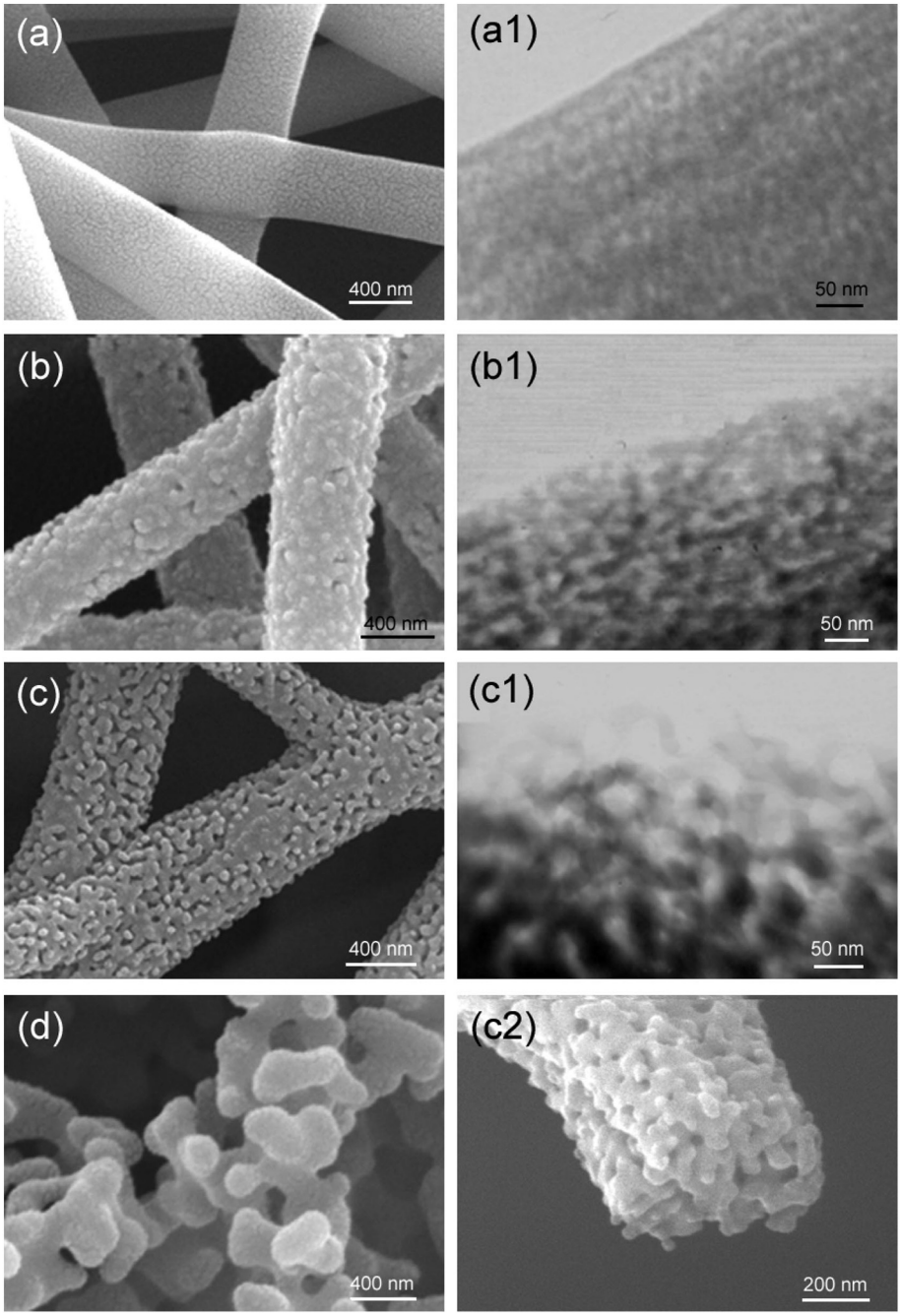

Fig. 8. SEM (a, b, c, and c2) and TEM (a1, b1, and c1) images of the calcined ES BG (silica) fibers. The nanofibers had 700 nm diameter with hierarchical porosity. Micro-porosity was reported to be 1.5 nm; the mesoporous diameter and morphology was altered by controlling the fibrous shrinkage to 0, 20, 40, and 60%: 0%-small irregular 3–6 nm mesopores (a and a1), 20%-irregular 3–15 nm mesopores (b and b1), 40%-worm-like macro/mesopores 30–70 nm (c and c1), 60%- cage-like macropores 450 nm (d and c2). The surface area as reported by BET analysis was 285, 218, and 156 m^2/g for 0%, 20%, and 40% shrunk samples respectively [21].

concentration below this led to the fabrication of the beaded fibers, and the concentration above this range made the solution too viscous to ES. These studies [21,57] indicate the importance of the molecular wt of the selected polymer on the concentration and resulting viscosity of the solution. To achieve adequate chain entanglements in ES solution, the relative concentration of the polymer should be used depending on the molecular wt of the polymer. Hong et al. [21] also reported that after keeping the concentration of polymer constant, the optimal ratio of surfactant: polymer wt ratio was 1–2. At lower ratios, the shrinkable capacity of the fiber was reduced or eliminated, but the coalesced fiber film was yielded.

5.6.3. *Effect of electric field strength*

To release a jet of fiber from the drop of liquid at the tip of the syringe, sufficient electric field strength is required to overcome surface tension. Xia et al. [57] reported that an electric field strength above 1.6 KV/cm was required to overcome the surface tension of the liquid; otherwise, fibers beaded. A field strength between 1.6 and 1.8 KV/cm fabricated stable fibers while the diameter was reduced as the field strength was increased. Also, the strength above 1.8 KV/cm resulted in extra electrostatic repulsive forces which made fibers unstable and increased their diameter.

Lu et al. [48] and Song et al. [66] ES 70SiO_2–30CaO mol% and BG fibers with SiO_2-CaO network (the composition of BG is not mentioned

Table 1
Various factors affecting ES of BGs studied in different published journal articles.
Abbreviations used in the table: *E*-electric field strength, D-distance between spinneret and collector, F-flow rate of the solution, V-viscosity of the solution, d-diameter of fibers, SA-surface area.

Authors	Type of glass	Polymer	Reported variables	Heat treatment	Diameter (d) Surface area (SA)	Factor affecting ES of BGs	Proposed applications
Hong et al. [21]	Silica fibers	PEO (M_n 2,000,000)	E: 10 KV D: 30 cm F: 3 ml/h	600 °C in air	d: 700 nm SA: 285, 218, 156 m^2/g for fibrous shrinkage of 0%, 20% and 40% respectively.	The concentration of polymer, the effect of surfactant, and protein adsorption	Protein adsorption
Allo et al. [26]	$70SiO_2$-26CaO-$4P_2O_5$ mol%	PCL	E: 15 KV D: 6 cm F:0.25 ml/h V: 25-35 mPa·s	- Composite fibers-PCL + BG	d: 320 ± 100 nm SA: -	Viscosity	Bone regeneration
Sakai et al. [19]	Silicate fibers		E: 15 KV D: - FR: -	60 °C overnight	d: Hundred nm to several μm SA: -	Bioactivity and cytotoxicity	Bone tissue engineering
Kim et al. [17]	$58SiO_2$–38CaO-4 P_2O_5 mol%	PVB	E: 1.5 KV/cm D: - F: 0.1 ml/h	700 °C for 3 h in air at a heating rate of 2 °C/min	d: 320 ± 87 nm SA: -	Bioactivity & cellular response	Bone regenerative medicine
Kim et al. [20]	$70SiO_2$-25CaO-$5P_2O_5$ mol%	PVB	E: 12 KV D: 8 cm F: 3 ml/h	700 °C for 3 h in air	d: 630–84 nm depending on sol concentration SA: -	The concentration of GPS, bioactivity, cellular response, 3D structure formulation	Osteogenic potential and applications in bone tissue engineering
Hong et al. [13]	$70SiO_2$-25CaO-$5P_2O_5$ mol%	PVA	E: 10 KV D: 30 cm F: 3 ml/h	600 °C in air for 4 h.	d: 500 nm SA: 276, 184, 141 m^2/g for small, middle and large pore fibers respectively	The concentration of polymer, the effect of surfactant, bioactivity, drug loading & release, wt loss of fibers.	Bone tissue engineering, wound health, and drug delivery
Hong et al. [22]	$70SiO_2$-25CaO-$5P_2O_5$ wt%	PEO (M_n = 2,000,000)	E: 10 KV D: 30 cm F: 3 ml/h	600 °C for 4 h	d: 500 nm SA: 148-166 m^2/g for 20,000 nm long fibers/ tubes.	Electric field strength, bioactivity, and drug loading & release	Drug delivery, scaffold for hard tissue repair, and wound healing
Lu et al. [48]	$70SiO_2$–30Cao mol%	PVA	E: 7-19 KV D: 15 cm F: 0.5 ml/h V: 1 Pa s	600 °C for 5 h in the air at a heating rate of 2 °C/min	d: 50–800 nm SA- 42.2 m^2/g	Electric field strength, mechanical properties	Bone tissue scaffolds
Xia et al. [57]	BG fibers with SiO_2-CaO-P_2O_5 network (the composition of BG is not mentioned in the article)	PVP (av mol wt-45,000)	E:1.8 KV/cm D: 5 cm F: -	As-spun fibers-37 °C for 1 day 600 °C for 5 h in air	d: 85 nm SA: -	Concentration and type of polymer solution, the addition of supplementary polymer, and bioactivity	Bone regeneration field
Poologasundarampillai et al. [58]	$70SiO_2$–30CaO mol%	–	E: 15 KV D: 1 cm F: 2.5 ml/h V: 0.56–0.95 Pa·s	60 °C for 72 h	d: 500-2000 nm SA-34.6 m^2/g	Bioactivity, cellular response, ease of packing in tooth extraction socket, confined compression testing.	Bone tissue regeneration
Gao et al. [60]	$47SiO_2$-$23B_2O_3$-25CaO-$5P_2O_5$ mol%	PVB (M_W = 144,000)	E: 7 KV D: 8 cm F:3.75 ml/h	700 °C for 3 h in air	d: 150–450 nm depending on the concentration of sol. SA- not given	The concentration of GPS, the effect of surfactant, and bioactivity.	Bone regeneration
Yamaguchi et al. [61]	Silicate fibers		E:10 KV D: 10 cm F: -	–	300–500 nm SA: -	Cellular response	Cell culture substrate and drug metabolism simulators
Choi et al. [62]	Silicate fibers	–		–		Electric voltage, wt reduction	Biomedical

(*continued on next page*)

Table 1 (*continued*)

Authors	Type of glass	Polymer	Reported variables	Heat treatment	Diameter (d) Surface area (SA)	Factor affecting ES of BGs	Proposed applications
			E: 16 KV D: 10 cm F: -		d: 200-400 nm SA: -		materials, fiber templates, reinforcing agents, and filters
Asgharnia et al. [63]	$29.4SiO_2$–$37.14CaO$-$32.06P_2O_5$–1.66MgO wt%	PVP (M_w = 25,000)	E: high D: 6 cm F: -	37 °C for one day 600 °C for 5 h in air	d: 156 nm SA-250 m^2/g	*In vitro* biomineralization, Wt reduction	Bioactivity
Song et al. [66]	BG with SiO_2-CaO network (the composition of BG is not mentioned in the article)	PVB	E: 10 KV D: 10 cm F: 0.6 ml/h	600 °C for 4 h in air	Inner d: 110 ± 30 nm Wall thickness: 120 ± 50 nm SA: -	Electric field strength, the distance between spinneret and collector, bioactivity	Drug delivery and bone regeneration
Wang et al. [69]	Silica nanotubes	PVP (M_w = 1,300,000)	E: 10 KV D: 15 cm F: -	200 °C for 2 h with heating rate 5 °C/min for annealing. 600 °C for 3 h	Outer d: 150-250 nm Wall thickness 40-60 nm SA: -	Phase separation leading to nanotube formation	–
Deliormanli [70]	13–93 (53% SiO_2-6Na_2O-12K_2O-5MgO-20CaO-4P_2O_5)	PVA (M_w = 88,000-97,000)	E: 20 KV D: 10 cm F: 1 ml/h	Aged at 60 °C, then dried at 120 °C for 1 day in air. Heat treatment at 250 °C for 4 h at 1 °C/min heating rate followed by a treatment at 625 °C for 4 h	464 ± 95 nm	Effect of surfactant on fiber morphology, bioactivity	Soft and hard tissue regeneration
Deliormanli [71]	45S5	PVA (M_w = 88,000-97,000)	E: 20 KV D: 8 cm F: 1 ml/h	Aged at 60 °C, dried at 120 °C for 1 day in air. Heat treatment at 300 °C for 4 h by a heating rate of 1 °C/min followed by a treatment at 600, 650, 680, and 700 °C for 2 h at 1 °C/min	280–335 ± 46 nm Fibers crystallized even before calcination.	Effect of calcination temperature on the crystallization of the fibers.	
Xie et al. [72]	Submicron BG tubes with SiO_2-CaO-P_2O_5 network (the composition of BG is not mentioned in the article)	PVP	$F_{mineral\ oil}$:0.05 ml/h F_{PVP}:1.5 ml/h	600 °C for 5 h in air	Inner diameter: 185-500 nm Outer diameter: 285-665 nm	Bioactivity, cell culture study, drug loading and delivery	Bone tissue engineering, topical drug or gene delivery
Deliormanli [56]	13–93 (53SiO_2-6Na_2O- 12K_2O-5MgO-20CaO-4P_2O_5 wt%) doped with Ce or Ga	PVA (M_w = 88,000-97,000)	E: 20 KV D: 10 cm F: 0.5 ml/h	Aged at 60 °C for 24 h, dried at 120 °C for 1 day in air. Heat treatment at 250 °C for 4 h at 1 °C/min heating rate followed by a treatment at 625 °C for 4 h	13–93: 464 ± 95 nm 13–93/Ce:361 ± 60 nm 13–93/Ga: 249 ± 43 nm	Bioactivity, cell cultures, antibacterial activity	Soft tissue engineering
Huang *et. al* [73]	70SiO_2-25CaO-5P_2O_5 mol% doped with either Eu or Tb	PVP	E: 10 KV D: 17 cm F: 1 ml/h	600 °C for 4 h in air	d:100-120 nm SA: Eu^{3+} = 188 m^2/g Tb^{3+} = 171 m^2/g	Cell viability by MTT, drug loading and delivery, luminescence	Drug carrier system
Durgalakshmi *et al* [74]	45S5	PVP	E: 10 and 15 KV D: 12 cm F: 0.2 & 0.3 ml/h	600 °C for 2 h in air	920-985 nm	Drug loading and delivery, MTT, bioactivity	Drug delivery, wound healing, and hard tissue applications

in the article) with the addition of PVA and polyvinyl butyrate (PVB), respectively. Lu et al. [48] reported that, as the voltage increased above the optimum voltage of 7 KV (for the distance between spinneret and collector = 15 cm), fibers with bead morphology were seen. Song et al. [66] reported that the electric voltage above an optimal value of 10 KV (for the distance between spinneret and collector = 10 cm) could not effectively deposit the fibers on the collector and voltage below 10 KV resulted in beaded fibers [66].

5.6.4. Effect of the concentration of glass precursor solution

Among the parameters that control fiber diameter, sol concentration is a dominant one [20]. The diameter of the fibers are seen to increase with the concentration of the sol [20,60], and the desired morphology of the fiber can be achieved by altering the concentration of the GPS [60]. Kim et al. [20] and Gao et al. [60] ES silicate ($70SiO_2$-25CaO-$5P_2O_5$ mol%) and borosilicate ($47SiO_2$-$23B_2O_3$-25CaO-$5P_2O_5$ mol%) BGs respectively with 10% PVB added equally to the solution. Both studies reported unstable, beaded fibers with randomly distributed diameters at a lower concentration of GPS around 0.2 M [60] and 0.25 M [20]. As the concentration of GPS increased from 0.2 M to 2 M [60] and 0.25 M to 1 M [20], the fibers lengthened, became more uniform and their diameter increased. Both studies [20,60] showed that increasing the concentration of GPS affects the fiber morphology.

5.6.5. Effect of feeding rate

Generally, the lower the feeding rate, the lesser the chances of bead formation and the smaller the diameter of the spun fibers [14]. Song et al. [66] stated 0.6 ml/h to be the optimal feeding rate for the solution for the production of BG hollow fibers with SiO_2-CaO network (the composition of BG is not mentioned in the article). A rate below this made it difficult to produce continuous fibers [66]. The relationship between fiber diameter and feeding rate of the solution has been depicted by studies showing higher diameter (0.5–2 μm) of the calcined fibers for higher feeding rates of 2.5 ml/h [58] than lower diameter fibers (50–800 nm) ES at lower feeding rates (0.5 ml/h) [48] for $70SiO_2$–30CaO mol% fibers.

5.6.6. Effect of the distance between spinneret and collector

Sufficient distance should be provided for the flight of the jet to reach the collector from the spinneret. It facilitates evaporation of the solvent, hardening of the polymer and promotes bead-free fibers [14]. Importance of optimum distance is evident from a study by Song et al. [66] for ES BG hollow fibers with SiO_2-CaO network (the composition of BG is not mentioned in the article); when the distance was kept lower than the observed optimum 10 cm distance, the process resulted in interconnected fibers. The correlation between the addition of polymer and distance between spinneret and collector was observed for $70SiO_2$–30CaO mol% fibers [48,58]. It was seen that with the addition of polymer (PVA), the distance reported was higher (15 cm) [48] for ES solution than without the addition of any polymer (1 cm) [58].

5.7. Induction of texture to the ES fibers

Similar to the way that fiber morphology is dependent on various factors (described in Section 5.6), textures can be induced (Fig. 8) to the ES fibers by application of various systems like polymer-surfactant, polymer-solvent, and surfactant structures in the solution. While Hong et al. [21] and Wang et al. [69] were able to fabricate porous and hollow silicate fibers by using polymer-surfactant and polymer-solvent systems respectively, Sakai et al. [19] and Yamaguchi et al. [61] fabricated solid silicate fibers in the absence of such systems.

5.7.1. Porosity

The assembly of the ES nano-fibers results in an interconnected macro-porous structure. The functionalization of the fibers can be further enhanced by induction of porosity in the fibers [13,21,60]. Nanoporous BG fibers can be synthesized using surfactant and surfactant-polymer prototypes as templates [21,60], but induction of porosity in the ES fibers is challenging [13,21,60].

Induction of porosity by surfactants is dependent on their ability to form micelles due to conformational entropy. But, in the process of ES, electric field strength stretches the surfactant and polymer molecules along the fiber axis which inhibits the formation of micelles [13,21,60]. Furthermore, the events of rapid evaporation of the solvent, swift formation of fibers, and immobility of the formed fibers on the collector, freeze the surfactant and polymer molecules in the stretched state [13,21,60]. The process of ES, in general, inhibits the endowment of porosity in the fibers due to the phenomenon mentioned above [13,21,60]. But when the as-spun fibers are removed from the collector and are then calcined in the furnace, the surfactant molecules in the removed fibers self-organize themselves in micelles with hydrophobic tails towards the center of the micelle and hydrophilic head outside to minimize the entropy [60]. Also, during calcination, the heat can overcome the limitations of outer forces stretching surfactant molecules allowing the surfactant molecules to relax and shrink due to high conformational entropy [13,21,60]. Relaxed surfactant molecules can undergo micellization and induce porosity in the fibers [13,21,60]. By regulating the shrinkage of the as-spun fibers [13,21] (Fig. 8) and the concentration of the surfactant (Fig. 9) [60], the mesopores' size can be altered. Gao et al. [60] demonstrated that mesoporosity could be tailored into the glass fibers with the addition of the triblock nonionic surfactant Pluronic F127 ($(PEO)_{100}$ - $(PO)_{65}$ - $(PEO)_{100}$); as the concentration of the surfactant was increased from 0% to 2%, the pore size was seen (by Scanning Electron Microscopy, SEM) to qualitatively enlarge and the diameter of the fiber reduced from 360 to 270 nm [60]. They reported 2 wt% of the surfactant F127 was optimum to design small diameter $47SiO_2$-$23B_2O_3$-25CaO-$5P_2O_5$ mol% fibers with larger mesopores; above this concentration, monolithic structures rather than fibrous constructs were reported. Hong et al. [21] used surfactant-polymer co-template along with ES to induce porosity on the ES silicate fibers. They used P123 surfactant in 1–4 wt% (after keeping the polymer concentration constant between 0.8 and 1.8 wt%) while maintaining surfactant: polymer wt ratio between 1 and 2 [21].

5.7.2. Hollow fibers

Nanotubes can further increase the surface area of the ES BG fibers along with increased bioactivity and drug loading capability [66]. Hollow fibers have also been used as sacrificial templates to grow nanotubes and can be functionalized by pre-dissolving functional components like nanoparticles and proteins to the ES solution [8]. When the right combination of viscous liquids is co-spinned using an inner and outer spinneret, co-axial fibers having both a core and a sheath of different materials can be manufactured. The core material can then be selectively removed using various techniques like solvent extraction and calcination to achieve nanotubes/hollow fibers [7].

The fiber morphologies can be controlled by altering the dominance between solvent evaporation and phase separation for polymers [69]. Hollow fibers are formed when solvent evaporation dominates the phase separation kinetics [69]. A study has shown that it is possible to ES co-axial fibers with a regular single nozzle spinneret [66]. The hollow fibers manufactured *via* this technique are the result of solvent evaporation and phase separation processes between the polymer (PVB) and silica precursor TEOS [66]. Due to the incompatibility of TEOS and PVB, TEOS tends to settle towards the center of the fiber, while PVB and calcium nitrate settling towards the periphery. Further, evaporation of TEOS helps to hollow out the fibers [66]. The wall of hollow fibers made with single spinneret tends to show homogeneous microstructure [66].

Hong et al. [22] demonstrated the fabrication of ultrathin ES BG fibers (Fig. 10) with both hollow cores and mesoporous walls by using a phase separation inducing agent along with the ES technique. Altering the ratio of the solvents (water and ethanol), they were able to

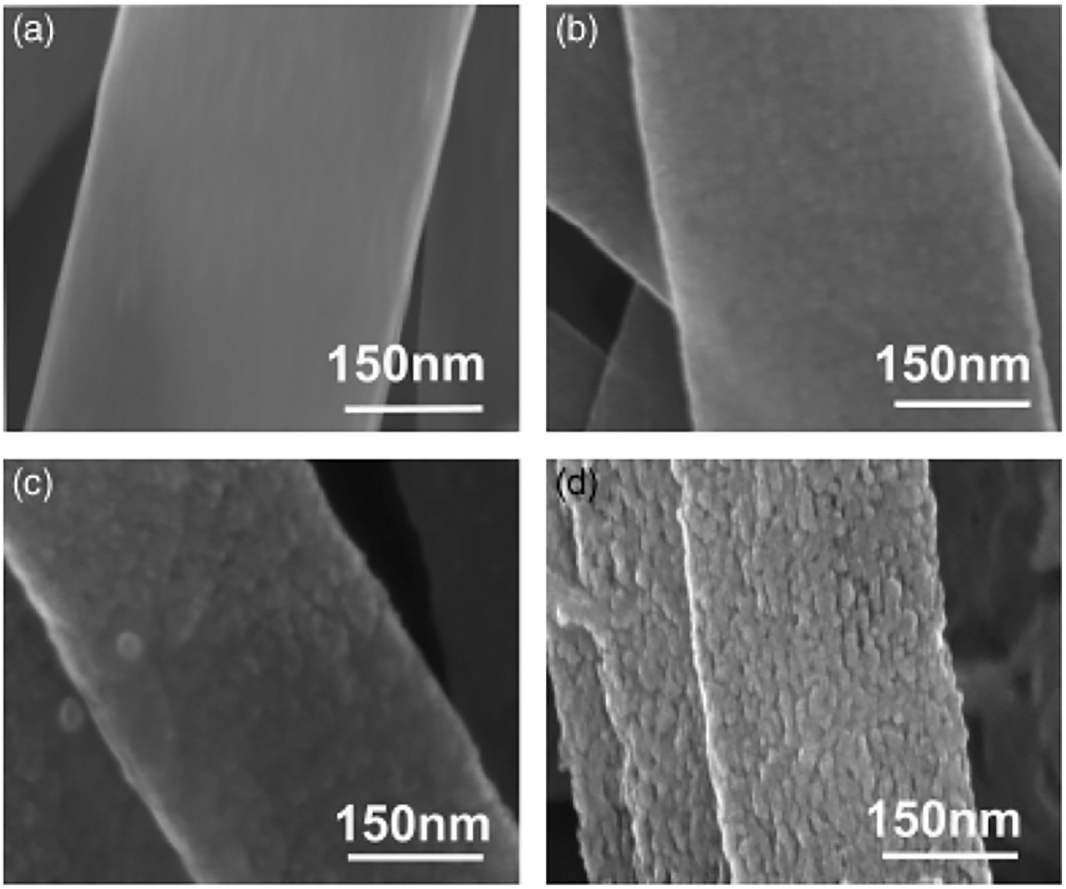

Fig. 9. Effect of concentration of surfactant (a-0%, b-1%, c-1.5%, and d-2%) on the morphology and fiber diameter of the fiber is depicted in the SEM images. As the concentration of the surfactant was increased the mesopores increased in size and fiber diameter reduced from 360 to 270 nm [60].

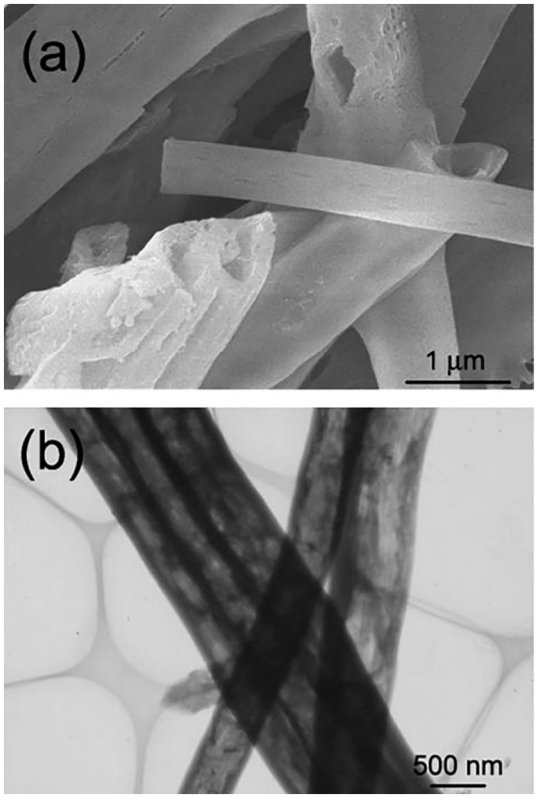

Fig. 10. SEM (a) and TEM (b) image of the hollow BG fiber [22].

compartmentalize the hollow fibers, but the fibers without compartments showed better incorporation of the drug [22].

Wang et al. [69] demonstrated that hollowness in the ES fibers could be achieved by partially hydrolyzing TEOS and making a sol-gel containing TEOS, PVP, ethanol and water. The fibers made by the glass/polymer composite as well as glass fibers (made after calcination of composite fibers) were hollow [69]. The inner wall was reported to be rough for composite fibers (pertaining to the rapid phase separation), while smooth for glass fibers; the outer wall was smooth for both composite and glass fibers [69]. The diameter of the hollow fibers can also be influenced by the molar ratio between water and TEOS; more of water allows TEOS to get hydrolyzed, which leads to the reduction in the diameter of the fibers. On the other hand, less of water allows more of TEOS to remain unhydrolyzed which leads to an increase in the diameter of the fibers [69].

5.8. Critical analysis of the factors

As listed in Table 1, various factors influence the process of ES and, subsequently, the morphology of the ES glass fibers. These factors are inter-related. For instance, the optimum electric field strength is required to overcome the surface tension of the solution (Section 5.6.3), which depends on the polymer and GPS composition. Primarily, GPS's composition dictates the application of the final ES product, but the viscosity of the solution (mostly a function of the polymer) plays an important role in carrying on the process of ES. Solution viscosity is primarily dependent on the concentration of the polymer [13,57] due to the high fluidity of GPS. Furthermore, electric field strength (Section 5.6.3), the viscosity of the solution (Section 5.6.1), and the concentration of both the polymer (Section 5.6.2) and GPS (Section 5.6.4)

affect the diameter and uniformity of the drawn fibers. It can be concluded that gaining from the trends that various ES factors follow as reported in the literature, the decision to finalize these factors depend upon the preferred composition, required morphology, desired orientation, and anticipated function.

6. *In vitro* bioactivity of glass fibers

Scaffolds for bone defects should be able to form a bone-like apatite layer when exposed to the biological environment [19]. Usually, for BGs, the dissolution-precipitation process leads to the formation of a HA-like layer. Dissolution of ions (Si, Ca, P, *etc.*) from the BG supersaturates the local environment with Ca and P, which eventually leads to the precipitation of Ca^{2+} and PO_4^{3-} species, leading to the formation of the HA-like layer [4,5,20]. Generally, the ES fibers provide a high surface area along with porosity which provides binding sites suitable for protein adsorption and cell attachments [58]. It has been shown for the ES nano-fibers (BG fibers with SiO_2-CaO-P_2O_5 network, the composition of BG is not mentioned in the article) that apatite preferred to nucleate and grow at the interconnected junctions (called 'cross-points') of BG nano-fibers in early stages of soaking in SBF (up to 6 h) [57]. It has been suggested that for the interconnected nano-fibers, the concentration of Ca is more at the cross-points compared to the fiber length due to the higher contact area of these fibers with surrounding fluid [57]. After prolonged soaking, the HA deposition is evident on the whole surface of the fibers joining the earlier deposition at cross-points (Fig. 11) [57].

The HA-like rod formation on the ES porous [13], solid [20], and hollow [22] fibers of compositions 70SiO_2-25CaO-5P_2O_5 mol%, 70SiO_2-25CaO-5P_2O_5 mol% and 70SiO_2-25CaO-5P_2O_5 wt% respectively after immersion in SBF is worth noting. All of the fibers [13,20,22] were calcined between 600 and 700 °C for 3-4 h in the air. Despite vast differences in the diameters of solid [20] and hollow [22] fibers (solid-84 nm and hollow-500 nm), these studies reported similar times of about one day for the HA-like rods to form. It is suggested that the hollowness of larger diameter fibers provided a higher surface area to deposit HA-like nanorods in a similar time frame as that of small diameter solid fibers [22]. When hollow [22] and solid [20] fibers are compared to the porous [13] fibers of similar composition in terms of HA-like rods formation, the porous fibers deposited these nanorods in about two days rather than one day (for the other two groups of fibers, solid and hollow). This can be attributed to the spatial restriction posed to the spherical particles depositing within the nanoporous structure of the fibers which are inhibited to further grow in the rod-like morphologies [13]. These studies also suggest that hollow [22] and porous [13] fibers of compositions 70SiO_2-25CaO-5P_2O_5 wt% and 70SiO_2-25CaO-5P_2O_5 mol% respectively with a diameter of ~500 nm calcined at 600 °C for 4 h in air exhibit different bioactivities due to their morphological differences.

Xie et al. [72] compared the *in vitro* bioactivity of the submicron BG tubes with SiO_2-CaO-P_2O_5 network (the composition of BG is not mentioned in the article) with solid BG fibers. Both samples were immersed in the SBF. They concluded that the mineralization process is enhanced for the BG tubes due to their hollowness (hence increased surface area) than the solid fibers. The mineralization process could only occur on the outer surface of the solid fibers but can occur outside and within the BG tubes. For BG tubes, HA-like material was noticed on Day 1 while the poorly crystallized deposits on the surface of solid fibers were witnessed on Day 3. Durgalakshmi et al. [74] tested the *in vitro* bioactivity of 45S5 ES hollow fibers by their immersion in the SBF. HA-like material was observed on the fibers by Day 3.

Deliormanli [70] performed *in vitro* bioactivity experiments on the ES 13–93 BG (53SiO_2-6Na_2O-12K_2O-5MaO-20CaO-4P_2O_5 wt%) fibers by immersing them in different ratios (0.5 mg/ml and 1 mg/ml) of amounts of SBF. The author reported that the formation of amorphous calcium phosphate or HA is affected by the fiber:SBF ratio [70]. Both groups showed the HA-like material formed on their surfaces on Day 1, but the group with 0.5 mg/ml ratio had a higher amount [70]. It was anticipated that higher BG:SBF ratio can increase the local pH which leads to the formation of calcium carbonate than HA [70].

In vitro bioactivity tests were also conducted on the ES 13–93 BG (53SiO_2-6Na_2O-12K_2O-5MaO-20CaO-4P_2O_5 wt%) fibers doped with either cerium, Ce or gallium, Ga [56]. The fibers were doped to exploit the benefits of cerium (Ce^{3+}) and gallium (Ga^{3+}) ions. Ce^{3+} has been proposed as a potential therapeutic agent, and BG foams containing nanoceria have shown increased osteoblastic differentiation of HMSCs

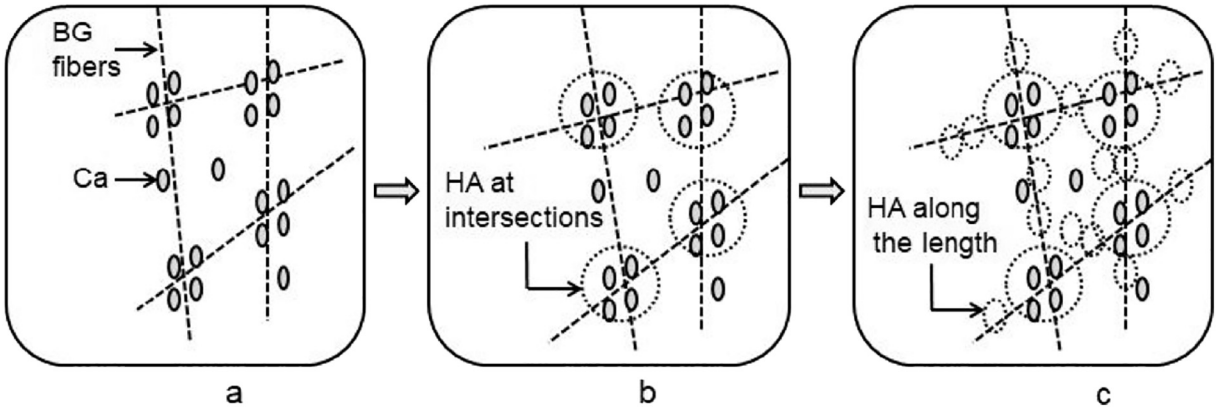

Fig. 11. Suggested scheme of bio-mineralization process for ES BG fibers [57]. The diagrammatic illustration is adapted from Xia et al. [57]. a- High Ca concentration can be seen at the points where BG fibers intersect each other; b- Due to high Ca concentration at the intersects, HA deposition can be seen earlier at these sites; c- After prolonged soaking, HA deposit all along the surface of the fibers joining HA at intersects. Studies have shown excellent bioactivity for ES 70SiO_2-25CaO-5P_2O_5 mol% [20], and 47SiO_2-23B_2O_3-25CaO-5P_2O_5 mol% [60] nano-fibers with rapid apatite formation than discs [20] and bulk glass [60] of similar composition. Also, BG fibers with SiO_2-CaO-P_2O_5 network (the composition of BG is not mentioned in the article) [57], manufactured by ES showed enhanced bioactivity than BG fibers made *via* a mechanical spinning technique [57]. Song et al. [66] showed that the bioactivity of the ES BG fibers could be further enhanced by inducing hollowness which provides additional sites for nucleation and growth of HA. Poologasundarampillai et al. [58] demonstrated rapid apatite formation on 3D "cotton-wool" like 70SiO_2–30CaO mol% fibers when soaked in SBF; they detected calcium phosphate within 1 h post-soaking. Gao et al. [60] highlighted that 47SiO_2-23B_2O_3-25CaO-5P_2O_5 mol% fibers maintained their fibrous structure even after five days of immersion in SBF which is an important criterion to be used as a scaffold in bone. Induction of porosity [13] and hollowness [22] in the fibers have been reported to further enhance the bioactivity of ES BG fibers. Morphological alterations within the multiple sized mesopores (small-3–5 nm, middle-3–16 nm, and large-32-65 nm pore size) has also been reported as a result of the formation of HA-like nanoparticles within these pores [13].

Table 2
In vitro bioactivity shown by various ES BG fibers-a comparison between their composition and morphology with the reported initiation of HA deposition after immersion in SBF.

Authors	Type of glass	Morphology	Fiber diameter	Immersion time in SBF when HA is first ascertained
Sakai et al. [19]	Silicate fibers	Solid	Several hundred nm to several μm	Seven days
Kim et al. [20]	$70SiO_2$-$25CaO$-$5P_2O_5$ mol%	Solid	630–84 nm	1 day
Hong et al. [13]	$70SiO_2$-$25CaO$-$5P_2O_5$ mol%	Pores	Av 500 nm	8 h
Hong et al. [22]	$70SiO_2$-$25CaO$-$5P_2O_5$ mol%	Hollow	500 nm	8 h
Xia et al. [57]	BG fibers with SiO_2-CaO-P_2O_5 network (the composition of BG is not mentioned in the article)	Solid	Av – 85 nm	6 h
Poologasundarampillai et al. [58]	$70SiO_2$–30CaO mol%	"Cotton-wool"	500-2000 nm	12 h
Gao et al. [60]	$47SiO_2$-$23B_2O_3$-$25CaO$-$5P_2O_5$ mol%	Pores	150–450 nm depending on the conc of sol.	1 day
S. Asgharnia et al. [63]	$29.4SiO_2$–$37.14CaO$-$32.06P_2O_5$–1.66MgO wt%	Solid	156 nm	12 h
Song et al. [66]	BG fibers with SiO_2-CaO network (the composition of BG is not mentioned in the article)	Hollow	Inner diameter – 110 ± 30 nm The thickness of the wall = 120 ± 50 nm	6 h
Deliormanli [70]	13–93 (53% SiO_2-$6Na_2O$-$12K_2O$-5MgO-20CaO-$4P_2O_5$)	Solid	464 ± 95 nm	1 day
Xie et al. [72]	Submicron BG tubes with SiO_2-CaO-P_2O_5 network (the composition of BG is not mentioned in the article)	hollow	Inner diameter: 185-500 nm Outer diameter: 285-665 nm	1 day
Deliormanli [56]	13–93 ($53SiO_2$-$6Na_2O$- $12K_2O$-5MgO-20CaO-$4P_2O_5$ wt%) doped with Ce or Ga	Solid	13–93 = 464 ± 95 nm 13–93/Ce:361 ± 60 nm 13–93/Ga:249 ± 43 nm	7–30 days
Durgalakshmi et al. [74]	45S5	Hollow	920-985 nm	3 days

(Human Mesenchymal Stem Cells) and collagen production [56]. Ga^{3+} is a known antibacterial and chemotherapeutic agent effective against bone resorption [56,75]. In the study [56], the *in vitro* bioactivity of the doped fibers were compared to the non-doped 13–93 fibers. It was seen that the presence of Ce^{3+}or Ga^{3+} reduced the second phase (calcium phosphate or crystalline HA) deposits on the surface of the fibers after 15 days. After 30 days, the doped fibers showed good bioactivity [56].

BGs are doped with various ions to utilize their beneficial effects towards a particular application [75,76]. Such additions to the BG compositions can enhance its function towards intended application but also alter the chemical structure of the glasses affecting their *in vitro* bioactivity [75,76]. Moghanian et al. [77] fabricated lithium substituted 58S BG in powder form to use the lithium's therapeutic properties. They found that the addition of Li to their composition delayed the formation of HA in SBF. It was also noted that the addition of Co, Zn, Mg, and Sr has also delayed HA formation [76,77]. Table 2 illustrates various studies conducted on the bioactive behaviour of ES BG nano-fibers comparing the composition and morphology of fibers with the reported initiation of HA deposition after immersion in SBF.

7. Cellular response

It has been suggested that cells show excellent response to ES fibrous scaffolds (also depending on the chemical composition of the scaffold) because these constructs resemble the native environment of the cells (ECM). Table 3 enlists various studies attempted for cellular response to ES BG fibers. Yamaguchi et al. [61] demonstrated that the human cell line HepG2 and Chinese hamster ovarian cells CHO-K1 proliferated and elongated faster on silicate fibers than on HA-pulp composite fiber sheet (HAPS)- a standard control for cell culture. The hepatocyte-specific functions were reported to be 5–10 times higher for silica fibers.

Sakai et al. [19] proved the application of ES ultrathin silicate fibers towards bone tissue engineering by demonstrating attachment and proliferation of the human osteoblastic MG63 cells to the ultrathin silicate fibers; apatite particle formation was also evident after immersing the fibers in SBF. Cells elongated and filled the spaces between the fibers. The number of intact mitochondria in the living cells also increased constantly over a period of five days signifying excellent mitochondrial activity and proliferation.

Kim et al. [17] compared BG $58SiO_2$–$38CaO$-$4P_2O_5$ mol% ES fibers-collagen nanocomposite scaffold with a collagen scaffold for functional activity of human osteoblastic MG63 cells by detecting ALP (alkaline phosphatase) levels. Cells seeded on the nanocomposite scaffold expressed higher amounts of ALP than on the collagen scaffold. Cells were also found to be growing and spreading favourably on the nanocomposite.

Poologasundarampillai et al. [58] demonstrated that 3D "cotton-wool" like $70SiO_2$–30CaO mol% fibers were not cytotoxic to MC3T3-E1 cells and further supported their attachment and proliferation. Attachment of osteoblasts to fibers was seen with the presence of filopodia (cytoplasmic projections seen in migrating cells) which indicates cellular attachment and proliferation. Clusters of cells were found to be immersed in ECM denoting capacity of these fibers to deposit ECM. A layer of crystalline particles was also observed on the attached cells, pointing towards their osteogenic capability [58].

Kim et al. [20] compared $70SiO_2$-$25CaO$-$5P_2O_5$ mol% ES fibers with both BG discs of the same composition and with PCL ES fibers. They found that cells spread actively on the nanofibrous surface with cytoplasmic extensions denoting osteogenic potential of the nano-fibers. It was also reported that cell viability of BG samples (slightly better for disc than fiber) was better than polymer fibers and BG fibers showed the highest expression of ALP which denotes osteogenic potential.

Xie et al. [72] fabricated hollow BG tubes with SiO_2-CaO-P_2O_5 network (the composition of BG is not mentioned in the article) and compared them with ES PCL fibers for cellular reactions (pre-osteoblastic MC3T3-E1 cells). After 3 days, the optical density of the cells seeded was lower on PCL fibers than the BG tubes. Also, after 3 days, MTT assay showed higher cell proliferation for BG tubes than PCL fibers. Durgalakshmi et al. [74] also demonstrated cytocompatibility of the hollow 45S5 ES fibers by MTT assay on MC3T3-E1 pre-osteoblast cell line.

Deliormanli [70] compared sintered scaffolds made by sol-gel ES BG fibers and melt-quench fabricated powder of same composition (13–93 glass, $53SiO_2$-$6Na_2O$-$12K_2O$-5MaO-20CaO-$4P_2O_5$ wt%) for their *in vitro* cytotoxicity. The cytotoxicity experiments were carried out on the mouse bone/calvaria pre-osteoblastic MC3T3-E1 (Sub-clone 4) cells using XTT (2,3-Bis-(2-Methoxy-4-Nitro-5-Sulfophenyl)-2H-Tetrazolium-

Table 3
Cellular response to ES BG fibers.

Authors	Type of glass	Cells line	Comparison	*In vitro* cellular assay	Results
Sakai et al. [19]	Silicate	Human osteoblastic MG63 cells	–	Cell morphology by fluorescence microscopy	Cells elongated and filled the spaces between the fibers.
				Mitochondrial activity by detecting the presence of dehydrogenase	Excellent mitochondrial activity.
Kim et al. [17]	$58SiO_2$–38CaO-4 P_2O_5 mol%	Human osteoblastic MG63 cells	BG fibers -collagen porous scaffold with collagen	Cell morphology with FESEM	Cells grew favourably.
				Functional activity with ALP detection.	Composite scaffold expressed higher levels of ALP than collagen alone.
Kim et al. [20]	$70SiO_2$-25CaO-5P_2O_5 mol%	Bone-marrow-derived stem cells	BG fibers and disc of the same composition	Cell viability with MTT and SEM.	BG fibers showed better cell viability and osteogenic potential with highest ALP detection.
				The osteogenic potential with ALP detection	
Poologasundarampillai et al. [58]	$70SiO_2$–30CaO mol%	MC3T3-E1 pre-osteoblast cell line	BG and PCL fibers –	Cell morphology on fibers' surface by SEM	Fibers not cytotoxic
				Cell viability by cell metabolic activity assay-MTT	Cellular attachment and proliferation.
					Induction of ECM deposition
					Crystalline particles on cell's surface indicating osteogenic potential
Yamaguchi et al. [61]	Silicate	Human cell line HepG2 and Chinese hamster ovarian cells CHO-K1	HA-pulp composite fiber sheet (HAPS)	Cell viability by crystal violet stain	Faster proliferation and elongation of cells
				Hepatocyte-specific functions-ammonia metabolism and albumin secretion rate	Better hepatocyte-specific function.
Deliormanli [70]	13–93 ($53SiO_2$-6Na_2O-12K_2O-5MgO-20CaO-4P_2O_5 wt%)	Mouse bone/calvaria MC3T3-E1 pre-osteoblast cells	Scaffolds of same composition prepared by melt-cast method	*In vitro* cytotoxicity with XTT assay. (2,3-Bis-(2-Methoxy-4-Nitro-5-Sulfophenyl)-2H-Tetrazolium-5-Carboxanilide)	No cytotoxicity and good biocompatibility
				Morphological observations of the cultured cells	
Xie et al. [72]	Submicron BG tubes with SiO_2-CaO-P_2O_5 network (the composition of BG is not mentioned in the article)	MC3T3-E1 pre-osteoblast cells	PCL fibers	Cell density	Higher on BG tubes
				MTT assay for cell proliferation	Higher optical density values for BG tubes on day 3
Deliormanli [56]	13–93 ($53SiO_2$-6Na_2O-12K_2O-5MgO-20CaO-4P_2O_5 wt%) doped with Ce or Ga	MC3T3-E1 pre-osteoblast cells	13–93 BG fibers	*In vitro* cytotoxicity with XTT assay. (2,3-Bis-(2-Methoxy-4-Nitro-5-Sulfophenyl)-2H-Tetrazolium-5-Carboxanilide)	No cytotoxicity
				Morphological observations of the cultured cells	Cells elongated, attached, spread and penetrated inside the porous structure of the scaffold.
Huang et al. [73]	$70SiO_2$-25CaO-5P_2O_5 mol% doped with Eu or Tb	L929 fibroblast cells		MTT assay	Low levels of cytotoxicity at higher concentration of fibers
Durgalakshmi et al. [74]	45S5	MC3T3-E1 pre-osteoblast cells	–	MTT assay	No cytotoxicity was noted, and cells showed viability

5-Carboxanilide) assay [70]. The results showed that cell viability of the fibrous scaffold was lower than the powder-based scaffold, but the difference was not statistically significant [70]. Both the groups were non-cytotoxic with well-spreading morphology [70]. The results of the study indicate the biocompatibility of the scaffolds [70]. 13–93 ES BG fibers were also doped with either Ce or Ga in a separate study [56]. The BG fibers were doped with these elements to utilize their therapeutic properties [56]. The 13–93 Ga or Ce doped ES fibrous BG scaffolds were compared with 13–93 ES fibrous BG scaffold for cytotoxicity using XTT assay on the mouse pre-osteoblastic MC3T3-E1 cell line [56]. It was shown that Ga and Ce doped fibrous scaffolds support cell attachment and proliferation [56]. The antibacterial properties of the scaffolds were also compared; it was found that although the ions are known antibacterial agents, the scaffolds did not show antibacterial effect using a zone inhibition test [56].

Huang et al. [73] made luminescent mesoporous ES BG fibers by doping ES fibers ($70SiO_2$-$25CaO$-$5P_2O_5$ mol%) with either europium (Eu^{3+}) or terbium (Tb^{3+}) ions at a doping concentration of 5 mol% of Ca^{2+}. These rare earth ions are proposed to be used towards bio-analytical sensors and bio-imaging set-ups [73]. The cytotoxicity of these fibers (in various concentrations) were evaluated using MTT assay on L929 fibroblast cells. The fibers were found to be non-cytotoxic, and the difference in the cell viability among various groups was negligible [73].

Although ES BG fibers have not been reported cytotoxic, there might be concerns regarding their toxicity due to the nano-dimensions [78] and excess release of dissolution products (dependent on their composition and degradability) [75]. It has been reported that nano-dimensions ≤ 0.25 μm in diameter and ≥ 8 μm in length have a carcinogenic potential [78]. In addition, the quick dissolution of these high surface area fibers can traverse the critical limit of ionic concentrations making them toxic to the local tissue [75]. The ES BG fibers should be tailored keeping these aspects into consideration.

8. Functional fibers

The fibers can be loaded with various biological payloads like drugs, dyes, enzymes and proteins as nanoparticles, nanowires and molecular species (usually termed as payload carriers) for different applications [8,13,21,22,79]. Hong et al. [21] showed the feasibility of protein (BSA-Bovine serum albumin) adsorption on porous silicate fibers with small pore fibers (3.8 nm pore size) showing slow BSA adsorption reaching equilibrium at 65 mg/g after 40 min, while large pore fibers (40 nm pore size) showing high BSA adsorption attaining equilibrium capacity of 130 mg/g after 40 min. Hong et al. [13,22] also reported the drug loading and release profiles of aminoglycoside antibiotic agent, gentamicin sulfate in the porous [13] and hollow [22] BG fibers. They stated that drug release and loading is dependent on the length of the hollow fibers' segments [22] and the pore size of the porous fibers [13]. They also demonstrated drug-burst behaviour and drug-controlled release process for porous fibers [13].

9. Conclusion

Bioactive glasses have been extensively used towards tissue engineering application. BGs can be formulated using melt-quench and sol-gel techniques to provide constructs with desired morphologies depending on the application that they are developed for. ES is a powerful technique to fabricate 1D nanostructured non-woven fibers. These fibers are advantageous for a wide variety of applications in the biomedical field such as bone regenerating materials, cell proliferation platforms, wound healing and drug delivery matrices, and functionalized payload carriers. One of the recent trends in constructing fibrous BG scaffolds is using the process of ES along with the sol-gel process. As compared to other sol-gel BG fiber formation methods (TASG, fiber drawing, and spraying), BG fibers fabricated using ES enhance the construct's architectural outcomes (which are conducive to cell's adhesion and proliferation). ES BG fibers can also be tailored to have customized morphology and textures to achieve desired results for biomineralization, osteogenesis, protein adsorption, and drug delivery applications. Though these constructs provide above-written advantages, they suffer from the inherent brittleness of glasses and cannot be used for load bearing applications. Researchers have tried to solve some of these problems with the addition of polymers to the final constructs making composite scaffolds.

The BG ES fibers have proved themselves equivalent if not better (in terms of *in vitro* bioactivity and cellular response) than the bulk powders and discs of the same composition. The possibility of hierarchical porous and fibrous morphology by ES BG fibers places them in the category of biomimetic constructs. Therefore, BG fibers have mostly been used towards osteogenesis. These morphologies further enhance the surface area of the constructs which can be useful to exploit their use as hemostats. Also, due to the biomimetic characteristics, their further extensive use is anticipated towards soft tissue repair and angiogenesis.

Acknowledgements

This research is supported by the Canadian Institute of Health Research (CIHR) Project [appl. # 366716. A novel approach to treating hemorrhage with mesoporous bioactive glasses].

References

[1] Hench L, Science JP-, 2002 U. 2002 Third-generation biomedical materials. Science. Sciencemag.Org 295. (doi:https://doi.org/10.1126/science.1067404).
[2] M.N. Rahaman, D.E. Day, B. Sonny Bal, Q. Fu, S.B. Jung, L.F. Bonewald, A.P. Tomsia, Bioactive glass in tissue engineering, Acta Biomater. 7 (2011) 2355–2373, https://doi.org/10.1016/j.actbio.2011.03.016.
[3] F. Quintero, J. Pou, R. Comesaña, F. Lusquiños, A. Riveiro, A.B. Mann, R.G. Hill, Z.Y. Wu, J.R. Jones, Laser spinning of bioactive glass nanofibers, Adv. Funct. Mater. 19 (2009) 3084–3090, https://doi.org/10.1002/adfm.200801922.
[4] J.R. Jones, Reprint of: review of bioactive glass: from Hench to hybrids, Acta Biomater. 9 (2013) 4457–4486, https://doi.org/10.1016/j.actbio.2015.07.019.
[5] L.L. Hench, The story of bioglass®, J. Mater. Sci. Mater. Med. 17 (2006) 967–978, https://doi.org/10.1007/s10856-006-0432-z.
[6] X. Yan, C. Yu, X. Zhou, J. Tang, D. Zhao, Highly ordered mesoporous bioactive glasses with superior in vitro bone-forming bioactivities, Angew. Chemie - Int. Ed. 43 (2004) 5980–5984, https://doi.org/10.1002/anie.200460598.
[7] D. Li, J.T. McCann, Y. Xia, M. Marquez, Electrospinning: a simple and versatile technique for producing ceramic nanofibers and nanotubes, J. Am. Ceram. Soc. 89 (2006) 1861–1869, https://doi.org/10.1111/j.1551-2916.2006.00989.x.
[8] D. Li, Y. Xia, Electrospinning of nanofibers: reinventing the wheel? Adv. Mater. 16 (2004) 1151–1170, https://doi.org/10.1002/adma.200400719.
[9] D. Li, Y. Xia, Fabrication of titania nanofibers by electrospinning, Nano Lett. 3 (2003) 555–560, https://doi.org/10.1021/nl034039o.
[10] D. Li, Y. Wang, Y. Xia, Electrospinning nanofibers as uniaxially aligned arrays and layer-by-layer stacked films, Adv. Mater. 16 (2004) 361–366, https://doi.org/10.1002/adma.200306226.
[11] Y. Wang, J.J. Santiago-Avil??s, Synthesis of lead zirconate titanate nanofibres and the Fourier-transform infrared characterization of their metallo-organic decomposition process, Nanotechnology 15 (2004) 32–36, https://doi.org/10.1088/0957-4484/15/1/006.
[12] J. Quirós, K. Boltes, R. Rosal, Bioactive applications for electrospun fibers, Polym. Rev. 56 (2016) 631–667, https://doi.org/10.1080/15583724.2015.1136641.
[13] Y. Hong, X. Chen, X. Jing, H. Fan, B. Guo, Z. Gu, X. Zhang, Preparation, bioactivity, and drug release of hierarchical nanoporous bioactive glass ultrathin fibers, Adv. Mater. 22 (2010) 754–758, https://doi.org/10.1002/adma.200901656.
[14] A.M. Jordan, V. Viswanath, S.-E. Kim, J.K. Pokorski, L.T.J. Korley, Processing and surface modification of polymer nanofibers for biological scaffolds: a review, J. Mater. Chem. B 4 (2016) 5958–5974, https://doi.org/10.1039/C6TB01303A.
[15] Y.F. Goh, I. Shakir, R. Hussain, Electrospun fibers for tissue engineering, drug delivery, and wound dressing, J. Mater. Sci. 48 (2013) 3027–3054, https://doi.org/10.1007/s10853-013-7145-8.
[16] P. Gupta, C. Elkins, T.E. Long, G.L. Wilkes, Electrospinning of linear homopolymers of poly(methyl methacrylate): exploring relationships between fiber formation, viscosity, molecular weight and concentration in a good solvent, Polymer (Guildf) 46 (2005) 4799–4810, https://doi.org/10.1016/j.polymer.2005.04.021.
[17] H.-W. Kim, J.-H. Song, H.-E. Kim, Bioactive glass nanofiber–collagen nanocomposite as a novel bone regeneration matrix, J. Biomed. Mater. Res. A 79A (2006) 698–705, https://doi.org/10.1002/jbm.a.30848.
[18] Pilar Sepulveda, Julian R. Jones, L.L. Hench, Characterization of melt-derived 45S5 and sol-gel-derived 58S bioactive Glassesle, J Biomed Mater Res B Appl Biomater 58

(2001) 734–740.
[19] S. Sakai, Y. Yamada, T. Yamaguchi, K. Kawakami, Prospective use of electrospun ultra-fine silicate fibers for bone tissue engineering, Biotechnol. J. 1 (2006) 958–962, https://doi.org/10.1002/biot.200600054.
[20] H.W. Kim, H.E. Kim, J.C. Knowles, Production and potential of bioactive glass nanofibers as a next-generation biomaterial, Adv. Funct. Mater. 16 (2006) 1529–1535, https://doi.org/10.1002/adfm.200500750.
[21] Y. Hong, H. Fan, X. Zhang, Synthesis and protein adsorption of hierarchical nanoporous ultrathin fibers, J. Phys. Chem. B 113 (2009) 5837–5842, https://doi.org/10.1021/jp9005444.
[22] Y. Hong, X. Chen, X. Jing, H. Fan, Z. Gu, X. Zhang, Fabrication and drug delivery of ultrathin mesoporous bioactive glass hollow fibers, Adv. Funct. Mater. 20 (2010) 1503–1510, https://doi.org/10.1002/adfm.200901627.
[23] L.L. Hench, J.K. West, The sol-gel process, Chem. Rev. 90 (1990) 33–72, https://doi.org/10.1021/cr00099a003.
[24] J.R. Jones, U. Jones, R. Julian (Eds.), Bio-Glasses an Introduction, A John Wiley & Sons, Ltd., Publication, Chichester, UK, 2012, pp. 29–44 (Department of Materials, Imperial College London, London, U Clare, Alexis G (New York State College of Ceramics, Alfred University, Alfred, NY).
[25] A. Rámila, F. Balas, M. Vallet-Regí, Synthesis routes for bioactive sol-gel glasses: Alkoxides versus nitrates, Chem. Mater. 14 (2002) 542–548, https://doi.org/10.1021/cm0110876.
[26] B.A. Allo, A.S. Rizkalla, K. Mequanint, Synthesis and electrospinning of ??-polycaprolactone-bioactive glass hybrid biomaterials via a sol-gel process, Langmuir 26 (2010) 18340–18348, https://doi.org/10.1021/la102845k.
[27] D. Levy, M. Zayat, The Sol-Gel Handbook, (2015), https://doi.org/10.1002/9783527670819.
[28] F. Hoffmann, M. Cornelius, J. Morell, M. Fröba, Silica-based mesoporous organic-inorganic hybrid materials, Angew. Chem. Int. Ed. 45 (2006) 3216–3251, https://doi.org/10.1002/anie.200503075.
[29] G. Turnbull, J. Clarke, F. Picard, P. Riches, L. Jia, F. Han, B. Li, W. Shu, 3D bioactive composite scaffolds for bone tissue engineering, Bioact. Mater. 3 (2018) 278–314, https://doi.org/10.1016/j.bioactmat.2017.10.001.
[30] G. Ratheesh, J.R. Venugopal, A. Chinappan, H. Ezhilarasu, A. Sadiq, S. Ramakrishna, 3D fabrication of polymeric scaffolds for regenerative therapy, ACS Biomater Sci. Eng. 3 (2017) 1175–1194, https://doi.org/10.1021/acsbiomaterials.6b00370.
[31] S. Kargozar, F. Baino, S. Hamzehlou, R.G. Hill, M. Mozafari, Bioactive glasses: sprouting angiogenesis in tissue engineering, Trends Biotechnol. 36 (2018) 430–444, https://doi.org/10.1016/j.tibtech.2017.12.003.
[32] F.Y. Hsu, M.R. Lu, R.C. Weng, H.M. Lin, Hierarchically biomimetic scaffold of a collagen-mesoporous bioactive glass nanofiber composite for bone tissue engineering, Biomed. Mater. 10 (2015) 25007, https://doi.org/10.1088/1748-6041/10/2/025007.
[33] J.D. Mackenzie, Applications of the sol-gel process, J. Non-Cryst. Solids 100 (1988) 162–168, https://doi.org/10.1016/0022-3093(88)90013-0.
[34] Y. Zhang, L. Chen, M. Shi, D. Zhai, H. Zhu, J. Chang, C. Wu, X. Zheng, J. Yin, Mesoporous bioactive glass nanolayer-modified zirconia coatings on Ti-6Al-4V with improved in vitro bioactivity, Int. J. Appl. Glas. Sci. 7 (2016) 216–228, https://doi.org/10.1111/ijag.12210.
[35] B. Guo, B. Lei, P. Li, P.X. Ma, Functionalized scaffolds to enhance tissue regeneration, Regen. Biomater. 2 (2015) 47–57, https://doi.org/10.1093/rb/rbu016.
[36] M. Trevelin Souza, P. Hatton, E. Dutra Zanotto, M. Santocildes Romero, L. Hidalgo Pitaluga, Electrospun F18 bioactive glass/PCL—poly (ε-caprolactone)—membrane for guided tissue regeneration, Materials (Basel) 11 (2018) 400, https://doi.org/10.3390/ma11030400.
[37] M.T. Souza, O. Peitl, E.D. Zanotto, A.R. Boccaccini, Novel double-layered conduit containing highly bioactive glass fibers for potential nerve guide application, Int. J. Appl. Glas. Sci. 7 (2016) 183–194, https://doi.org/10.1111/ijag.12208.
[38] D. Moura, M.T. Souza, L. Liverani, G. Rella, G.M. Luz, J.F. Mano, A.R. Boccaccini, Development of a bioactive glass-polymer composite for wound healing applications, Mater. Sci. Eng. C 76 (2017) 224–232, https://doi.org/10.1016/j.msec.2017.03.037.
[39] J.J. Santiago-Aviles, Y. Wang, R. Furlan, I. Ramos, Synthesis and characterization of micro/nanoscopic Pb(Zr 0.52 Ti 0.48)O 3 fibers by electrospinning, Appl. Phys. A Mater. Sci. Process. 78 (2004) 1043–1047, https://doi.org/10.1007/s00339-003-2152-2.
[40] R.F. Brown, D.E. Day, T.E. Day, S. Jung, M.N. Rahaman, Q. Fu, Growth and differentiation of osteoblastic cells on 13–93 bioactive glass fibers and scaffolds, Acta Biomater. 4 (2008) 387–396, https://doi.org/10.1016/j.actbio.2007.07.006.
[41] F.T. Wallenberger, J.C. Watson, L. Hong, Glass Fibers, ASM Hanb, vol. 21, 2001, pp. 27–34, , https://doi.org/10.1361/asmhba0003353.
[42] J.E. Spruiell, J.L. White, Structure development during polymer processing: studies of the melt spinning of polyethylene and polypropylene fibers, Polym. Eng. Sci. 15 (1975) 660–667.
[43] D.C. Clupper, L.L. Hench, Crystallization kinetics of tape cast bioactive glass 45S5, J. Non-Cryst. Solids 318 (2003) 43–48, https://doi.org/10.1016/S0022-3093(02)01857-4.
[44] H. Luo, Y. Zhang, G. Li, J. Tu, Z. Yang, G. Xiong, Z. Wang, Y. Huang, Y. Wan, Sacrificial template method for the synthesis of three-dimensional nanofibrous 58S bioglass scaffold and its in vitro bioactivity and cell responses, J. Biomater. Appl. 32 (2017) 265–275, https://doi.org/10.1177/0885328217715784.
[45] H. Luo, W. Li, H. Ao, G. Li, J. Tu, G. Xiong, Y. Zhu, Y. Wan, Preparation, structural characterization, and in vitro cell studies of three-dimensional SiO2–CaO binary glass scaffolds built ofultra-small nanofibers, Mater. Sci. Eng. C 76 (2017) 94–101, https://doi.org/10.1016/j.msec.2017.02.134.
[46] R.L. Oréfice, L.L. Hench, A.E. Clark, A.B. Brennan, Novel sol-gel bioactive fibers, J. Biomed. Mater. Res. 55 (2001) 460–467, https://doi.org/10.1002/1097-4636(20010615)55:4 < 460::AID-JBM1037 > 3.0.CO;2-3.
[47] R.Z. Domingues, A.E. Clark, A.B. Brennan, A sol-gel derived bioactive fibrous mesh, J. Biomed. Mater. Res. 55 (2001) 468–474, https://doi.org/10.1002/1097-4636(20010615)55:4 < 468::AID-JBM1038 > 3.0.CO;2-T.
[48] H. Lu, T. Zhang, X.P. Wang, Q.F. Fang, Electrospun submicron bioactive glass fibers for bone tissue scaffold, J. Mater. Sci. Mater. Med. 20 (2009) 793–798, https://doi.org/10.1007/s10856-008-3649-1.
[49] H. Luo, Y. Zhang, Z. Wang, Z. Yang, J. Tu, L. Zhenhua, Y. Fanglian, G. Xiong, Y. Wan, Constructing three-dimensional nanofibrous bioglass/gelatin nanocomposite scaffold for enhanced mechanical and biological performance, Chem. Eng. J. 210–221 (2017), https://doi.org/10.1016/j.cej.2017.05.115.
[50] M.G. McKee, J.M. Layman, M.P. Cashion, T.E. Long, Phospholipid nonwoven electrospun membranes, Science 311 (2006) 353–355, https://doi.org/10.1126/science.1119790 (80-.).
[51] D. Li, Y. Xia, Direct fabrication of composite and ceramic hollow nanofibers by electrospinning, Nano Lett. 4 (2004) 933–938, https://doi.org/10.1021/nl049590f.
[52] S. Megelski, J.S. Stephens, D. Bruce Chase, J.F. Rabolt, Micro- and nanostructured surface morphology on electrospun polymer fibers, Macromolecules 35 (2002) 8456–8466, https://doi.org/10.1021/ma020444a.
[53] A. Patlolla, G. Collins, T. Livingston Arinzeh, Solvent-dependent properties of electrospun fibrous composites for bone tissue regeneration, Acta Biomater. 6 (2010) 90–101, https://doi.org/10.1016/j.actbio.2009.07.028.
[54] J. Yuh, J.C. Nino, W.M. Sigmund, Synthesis of barium titanate (BaTiO3) nanofibers via electrospinning, Mater. Lett. 59 (2005) 3645–3647, https://doi.org/10.1016/j.matlet.2005.07.008.
[55] Y. Wu, L.L. Hench, J. Du, K.-L. Choy, J. Guo, Preparation of hydroxyapatite fibers by electrospinning technique, J. Am. Ceram. Soc. 87 (2005) 1988–1991, https://doi.org/10.1111/j.1151-2916.2004.tb06351.x.
[56] A.M. Deliormanlı, Electrospun cerium and gallium-containing silicate based 13-93 bioactive glass fibers for biomedical applications, Ceram. Int. 42 (2016) 897–906, https://doi.org/10.1016/j.ceramint.2015.09.016.
[57] W. Xia, D. Zhang, J. Chang, Fabrication and in vitro biomineralization of bioactive glass (BG) nanofibres, Nanotechnology 18 (2007), https://doi.org/10.1088/0957-4484/18/13/135601.
[58] G. Poologasundarampillai, et al., Cotton-wool-like bioactive glasses for bone regeneration, Acta Biomater. 10 (2014) 3733–3746, https://doi.org/10.1016/j.actbio.2014.05.020.
[59] S. Madhugiri, W. Zhou, J.P. Ferraris, K.J. Balkus, Electrospun mesoporous molecular sieve fibers, Microporous Mesoporous Mater. 63 (2003) 75–84, https://doi.org/10.1016/S1387-1811(03)00433-5.
[60] C. Gao, Q. Gao, X. Bao, Y. Li, A. Teramoto, K. Abe, Preparation and in vitro bioactivity of novel mesoporous borosilicate bioactive glass nanofibers, J. Am. Ceram. Soc. 94 (2011) 2841–2845, https://doi.org/10.1111/j.1551-2916.2011.04434.x.
[61] T. Yamaguchi, S. Sakai, K. Kawakami, Application of silicate electrospun nanofibers for cell culture, J. Sol-Gel Sci. Technol. 48 (2008) 350–355, https://doi.org/10.1007/s10971-008-1822-0.
[62] S. Choi, S.G.O.O. Lee, Silica nanofibers from electrospinning/sol-gel process, J. Mater. Sci. Lett. (2003) 891–893, https://doi.org/10.1023/A:1024475022937.
[63] S. Asgharnia, P. Alizadeh, Synthesis and characterization of SiO2-CaO-P2O5-MgO based bioactive glass and glass-ceramic nanofibres by electrospinning, Mater. Lett. 101 (2013) 107–110, https://doi.org/10.1016/j.matlet.2013.03.089.
[64] M.G. McKee, G.L. Wilkes, R.H. Colby, T.E. Long, Correlations of solution rheology with electrospun fiber formation of linear and branched polyesters, Macromolecules 37 (2004) 1760–1767, https://doi.org/10.1021/ma035689h.
[65] E.J. Lee, S.H. Teng, T.S. Jang, P. Wang, S.W. Yook, H.E. Kim, Y.H. Koh, Nanostructured poly(ε-caprolactone)-silica xerogel fibrous membrane for guided bone regeneration, Acta Biomater. 6 (2010) 3557–3565, https://doi.org/10.1016/j.actbio.2010.03.022.
[66] B. Song, L. Wu, C. Wu, J. Chang, Preparation of hollow bioactive glass nanofibers by a facile electrospinning method, Biomed. Glas. 1 (2015) 136–139, https://doi.org/10.1515/bglass-2015-0013.
[67] A.R. Boccaccini, M. Erol, W.J. Stark, D. Mohn, Z. Hong, J.F. Mano, Polymer/bioactive glass nanocomposites for biomedical applications: a review, Compos. Sci. Technol. 70 (2010) 1764–1776, https://doi.org/10.1016/j.compscitech.2010.06.002.
[68] H. Fong, I. Chun, D.H. Reneker, Beaded nanofibers formed during electrospinning, Polymer (Guildf) 40 (1999) 4585–4592, https://doi.org/10.1016/S0032-3861(99)00068-3.
[69] W. Wang, et al., A novel method to fabricate silica nanotubes based on phase separation effect, J. Mater. Chem. 20 (2010) 9068, https://doi.org/10.1039/c0jm02120b.
[70] A.M. Deliormanli, Preparation, in vitro mineralization and osteoblast cell response of electrospun 13-93 bioactive glass nanofibers, Mater. Sci. Eng. C 53 (2015) 262–271, https://doi.org/10.1016/j.msec.2015.04.037.
[71] A.M. Deliormanli, Preparation and in vitro characterization of electrospun 45S5 bioactive glass nanofibers, Ceram. Int. 41 (2014) 417–425, https://doi.org/10.1016/j.ceramint.2014.08.086.
[72] J. Xie, E.R. Blough, C.H. Wang, Submicron bioactive glass tubes for bone tissue engineering, Acta Biomater. 8 (2012) 811–819, https://doi.org/10.1016/j.actbio.2011.09.009.
[73] S. Huang, X. Kang, Z. Cheng, P. Ma, Y. Jia, J. Lin, Electrospinning preparation and drug delivery properties of Eu3 + /Tb3 + doped mesoporous bioactive glass nanofibers, J. Colloid Interface Sci. 387 (2012) 285–291, https://doi.org/10.1016/j.jcis.

2012.08.004.
[74] D. Durgalakshmi, S. Balakumar, Phase separation induced shell thickness variations in electrospun hollow bioglass 45S5 fiber mats for drug delivery applications, Phys. Chem. Chem. Phys. 17 (2015) 15316–15323, https://doi.org/10.1039/c5cp01738f.
[75] G. Kaur, O.P. Pandey, K. Singh, D. Homa, B. Scott, G. Pickrell, A review of bioactive glasses: their structure, properties, fabrication and apatite formation, J. Biomed. Mater. Res. A 102 (2014) 254–274, https://doi.org/10.1002/jbm.a.34690.
[76] A. Hoppe, N.S. Güldal, A.R. Boccaccini, A review of the biological response to ionic dissolution products from bioactive glasses and glass-ceramics, Biomaterials 32 (2011) 2757–2774, https://doi.org/10.1016/j.biomaterials.2011.01.004.
[77] A. Moghanian, S. Firoozi, M. Tahriri, Synthesis and in vitro studies of sol-gel derived lithium substituted 58S bioactive glass, Ceram. Int. 43 (2017) 12835–12843, https://doi.org/10.1016/j.ceramint.2017.06.174.
[78] F. Stanton, M. Layard, A. Tegeris, A. Smith, E. Miller, M. May, Relation of Particle Dimension to Carcinogenicity in Amphibole and Other Fibrous Minerals, vol. 67, (2001), pp. 965–975.
[79] S. Ur Rahman, M. Nagrath, S. Ponnusamy, P.R. Arany, Nanoscale and macroscale scaffolds with controlled-release polymeric systems for dental craniomaxillofacial tissue engineering, Materials (Basel) 11 (2018), https://doi.org/10.3390/ma11081478.